CHALMERS

The development of methods to analyze pharmacoMRI data

Master of Science Thesis

YUAN WANG
SHANGWENYAN GONG

The development of methods to analyze pharmacoMRI data

YUAN WANG
Telephone + 46 (0)705538162
Department of Communication Engineering

SHANGWENYAN GONG
Telephone +46 (0)735694126
Department of Biomedical Engineering

Supervisors:
RAIMO JOENSUU
R &D Personalized Healthcare and Biomarkers
AstraZeneca
SE-431 83 Mölndal
Sweden

ARTUR CHODOROWSKI
Chalmers University of Technology
SE-412 96 Göteborg
Sweden

Examiner: MIKAEL PERSSON
Chalmers University of Technology
SE-412 96 Göteborg
Sweden
Göteborg, Sweden, September 2011

Acknowledgements

Möndal, September 30, 2011

Yuan Wang and Shangwenyan Gong

Abstract

Appetite-controlling drugs are anti-obesity pharmacological agents that reduce or control weight. However, the mechanism of the drug is sometimes poorly understood. In this work, methods were developed to analyze data from small rodents acquired by pharmacological magnetic resonance imaging (phMRI) technique, to identify the brain regions responded to the drug-challenge and to qualify the response. Two datasets were analyzed, one is based on signal intensity (dataset A) and the other is T_2* map (dataset B).

  The method can be divided into two parts: Data processing and Statistical analysis.

  Data processing aimed at removing artifacts caused by field inhomogeneity, system drift and animal motion effect. Four approaches were developed and tested: Filter, rigid-body, overlay and external reference phantom methods. The overlay method was the most effective in eliminating the artifacts. Standard spatial processing steps were then used for motion correction.

  In the statistical analysis, Time-bin, shuffle and clearance model methods were implemented. The clearance model method is the most sensitive to locate the brain activation areas by generating a new dataset named sample group.

  The change of relative cerebral blood volume, which represents the compound effect, was calculated in the activated regions.

  The analysis method developed in this project identified the drug-induced brain activation areas with statistically significant p-value in both datasets, and the dose effect was observed in the dataset A.

Key words: Appetite-controlling drug, phMRI, clearance, relative cerebral blood volume

Chapter 1 **Introduction**

1.1 Magnetic Resonance Imaging

Felix Bloch and Edward Mills Purcell (1-3) discovered the chemical technique known as the nuclear magnetic resonance (NMR) which forms the root to the imaging technique, (magnetic resonance imaging, MRI.

The NMR signal originates from nuclei with non-zero magnetic moment which, when placed in a magnetic field (B0) will align themselves to the same or opposite direction with respect to the external field. The magnetic moments, also called as spins, are not exactly aligned with the magnetic field but will precess around it at a specific frequency which is determined by the magnetic field strength and the type of nucleus. This precession frequency is called Larmor frequency. There will also be an excess of spins in the orientation which has the lowest energy level and these spins combined to form a called a macroscopic magnetization.

Radio frequency (4) irradiation at a Larmor frequency forces the individual spins to precess coherently and the macroscopic magnetization to deviate from the direction of the static magnetic field. When the RF irradiation is turned off the magnetization will return back to its original state, and energy will be released which can be detected by the scanners RF coils.

To enable imaging, extra gradient magnetic field is added on top of the static field, which results in resonance frequency to vary in space in a pre-determined manner. The RF pulses with a specified frequency range can be used to excite a slice. Moreover, additional gradients in the so called phase and frequency encoding directions are applied which will enable to identify the signal's spatial positions and hence enable imaging.

Brain is an organ with a high density (ca. 100M) of hydrogen nuclei which has a high gyro magnetic ratio, whereupon a high NMR sensitivity. Compared to single photon emission computed tomography (CT), electroencephalogram (EEG) or positron emission tomography (PET), MRI has the advantage of a relatively high spatial resolution (<1mm), unambiguous signal localization and the absence of ionization radiation.

1.2 Pharmacological MRI

Pharmacological MRI (phMRI) is a specific MRI technique aimed at investigation of brain response to pharmacological stimulus, and it covers studies of neurotransmitter systems, psychiatric and neurological conditions, and drug-induced brain activities. With phMRI, it is possible to locate and quantify functional effects of drugs which make it a desirable tool for pharmaceutical research.

phMRI is based on the established theory that cerebral physiological functionality is directly reflected by the energy metabolism, or in another word, the localized blood supply in neural tissue (5).

There are several techniques for performing a phMRI experiment, but the typical characteristic for all of them is a repeated scanning over a long time to follow the spatial-temporal patterns of signal intensity. By far the most commonly used measurement techniques in phMRI are relative cerebral blood volume (rCBV), blood oxygenation level-dependent (BOLD), and T1-based cerebral blood flow (CBF) (6). BOLD signal infers regional oxygen consumption, but the signal is also a complex function of blood flow and volume which makes quantification challenging. CBF signal changes can be measured by using arterial spin labeling, but it requires extra hardware and pulse sequences so the whole brain coverage is challenging (7).

Cerebral blood volume is defined as blood volume (in milliliter) per 100 mL brain tissue. Instead of measuring CBV in absolute values, rCBV is usually measured as the ratio of the area under the contrast agent concentration curve relative to that in standard tissue (8).

The rCBV method is more sensitive than BOLD and CBF methods but it requires the use of exogenous contrast agent, for instance, iron oxide with long blood half-life (6), rCBV changes in

activation site can be as large as 30%, but with appetite controlling compounds the changes can be expected to be in the order of 7% (7).

Studies of drugs have been carried out by phMRI, such as by heroin (9), cocaine (10-12), nicotine (13-14), caffeine (15-16), fenfluramine (17), ketamine (18) and apomorphine (19). phMRI has also been used in studying diseases like drug-abuse, depression, Parkinson's disease and obesity.

1.3 The Purpose of this study

This study aimed at developing and testing a post-processing method to identify rat brain regions which respond to appetite regulating compounds, and to quantify their dose effect. The developed software was tested for two different kinds of animal data which had been acquired separately. Hereafter referred as A and B. The improved sensitivity to detect the compound effect, which is as small as a drift upon control data, is the main significance of our method.

Chapter 2 **Challenges and Limitations**

The compound effect in our study is expected to be a drift-like change of the signal, which is difficult to detect due system and subject-dependent noise (7).Challenges that limit the sensitivity of a phMRI study to detect drug response are discussed.

Magnetic field inhomogeneities

Magnetic susceptibility differences near tissue/air interface, particularly in brain regions near air cavities will introduce magnetic field inhomogeneities and signal loss. This type of inhomogeneity is referred to as macroscopic static field inhomogeneity, since the alternation of main magnetic field arises in relatively large areas (20). The effect is particularly large with imaging sequences which are designed to be sensitive to susceptibility variations.

Statistical magnetic field inhomogeneities will lead to two main problems. First is signal loss due to intravoxel dephasing. Second is image distortion, which means dislocation of pixels in the image (21). RF inhomogeneity in the transmit field will also cause variations in the excitation flip angle and variations in position-dependent contrast. Moreover, an inhomogeneous receiver coil's sensitivity profile will cause the signal intensity to be position-dependent. This is not so much of an issue in a functional study unless the subject moves during the scan. In that case, the time series signal-intensity will be modified by the motions and there are no ready-made tools to remove this type of artifact.

Thermal drift

During MR scan, electronic circuitry and temperature-controlling blowers will introduce thermal variation and thus induce field gradient drift. Image distortion will appear in and the animal position in acquired images will have a slow drift in time series.

Subject motion

Subject movement is a well-known problem in time-series acquisition for phMRI study. It will result in signal intensity fluctuations over time and space. Subject respiration, cardiac activity, and metabolic reactions like blood flow can cause motion artifacts, which may all mimic compound effects. Although restraining subject's movement can help to reduce these artifacts, it can raise the subject tension and discomfort. Thus it is a challenging task to keep subject stable over long time scanning (22).

To improve the sensitivity of compound effect detection, our studies focus on development and optimization of methods to reduce noises and artifacts from above factors yet maintain useful information.

Chapter 3 **Materials and Methods**

This chapter describes the data acquisition and analysis methods which were developed in this work. Figure 3. 1 shows the data processing and analysis work frame which was applied to two datasets (A, B) where both the acquisition methods and the compound where different from each other. This work can be divided into two parts data processing and statistical analysis. Data processing contains signal intensity correction, spatial processing and T_2* map generation. Statistical analysis is implemented by using three different methods: SPM standard analysis, shuffle and clearance model methods.
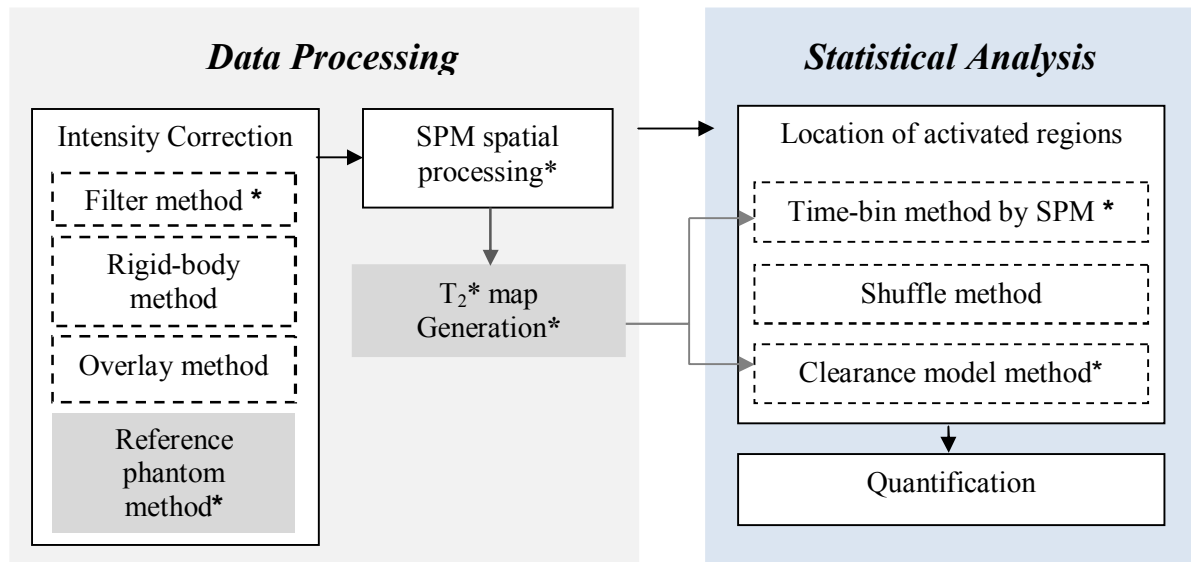
Figure 3. 1 The analysis steps. All the steps within the white regions are applied for the dataset A. Procedures with '*' and in the gray regions are carried out for dataset B.

3.1 In-vivo Animal phMRI

A 9.4T magnetic resonance imaging instrument was used for the data acquisition (Bruker Biospec 94/20, Bruker Cooperation, Germany). Animals (rats) were anaesthetized and scanned in the magnet with temperature control and freely breathing (1:1, air: oxygen). The acquisitions were slightly different for the two datasets.

Dataset A

This dataset consists of MR scans of 44 female rats' brains. MR contrast media Ferumoxide (1mL/kg i.v. ≡ Fe 0.2mmol/kg) was infused via tail vein. Substance A was administered 1mL/kg via jugular vein.

The animals were divided into four groups: 0.9 mM substance group (11 animals); 4.8 mM group (12 animals), 28 mM group (11 animals), and the vehicle group (10 animals), H_2O was used as a vehicle solution.

The scanning parameters were: 3D gradient echo=1; repetitions time=42.6; echo time=13ms; flip angle=12; acquisition matrix= 64x128x24; field of view=3.0x3.0x1.3cm; number of time points=50.

Contrast agent (CA) infusion finished at time point 10 and the substance was infused between the time points 17and 20. The compound effect is expected after 21st time point. Time points 1 to 4 from the baseline were used for the ΔrCBV calculation.

Dataset B

Six rats were divided equally into compound and vehicle group. The preparation was the same as dataset A.
The scanning parameters were:
  3D gradient echo=8; repetitions time=75; echo time (TE) /echo interval(ΔTE)=2.1/3.1 ms; flip angle=16; acquisition matrix= 128x64x32; field of view=3.0x3.0x1.6cm; number of time points=100. Contrast agent (CA) was given at time point 10 and the substance was infused at time point 40. Substance here is referred to vehicle (saline) or compound.
  To improve the data quality, the external reference phantoms were scanned together with animals to correct confounds introduced by signal drift [Table 1].

Table 1
Phantom Preparation. Two phantoms were prepared scanned with animals separately.

Phantom	Composition	Preparation	Placement
1	Feraheme (USPIO in H_2O, 15ppm), Agarose(3%)	Magnetic stir USPIO solution and preheat in 50 degree centigrade Dissolve 3% Agarose in the solution, and cool in room temperature	Injected in a semi-circular glass tube placed around animal nose
2	Silicone gel	None	Injected in the animal ear

3.2 Software and Tools

Several well-developed software were used in our study for data processing:
  Para Vision (Bruker BioSpin, German): Para Vision is a tool for data-acquisition from MR instrument, as well as encode, reconstruct and archive data for following processing. It is used along with pre-clinical MR imaging and spectroscopy.
  Statistical Parametric Mapping (SPM8, Wellcome Trust Centre for Neuroimaging, London) Statistical Parametric Mapping (SPM) refers to software for human-brain functional imaging data processing, including preprocessing and statistical analysis. In spatial processing, image sequences are realigned, normalized to a template, and smoothed. In statistical analysis, General Linear Model (GLM) is used to describe property for each animal.
  Matlab (R2010b, MathWorks, U.S.A):The the coding platform for the whole project is Matlab. SPM8 is a Matlab-based software. The methods developed in our study for data processing and analysis were also coded and tested in Matlab.

3.3 Data Processing

3.3.1 Intensity Correction

The animal (or human) can move during a long data acquisition time, therefore all advanced functional MRI analysis packages contain motion correction algorithms. However, if a surface coil is used with an inhomogeneneous sensitivity pattern, the motion can also cause signal intensity changes which normally cannot be corrected by using standard software packages. Here data has been acquired by the vendor's surface brain array coil and the time series data contained motion-induced intensity changes which were uncorrectable by standard techniques. In this work, three different techniques were developed and tested to correct it: Filter method, Rigid-body method and Overlay method.

3.3.1.1 Filter Method

Filter method basically works by using a filter to smooth the time-intensity curve for each pixel in a brain. In this work, the filter should remove all the motion induced signal intensity variation, but retain the signal changes which are caused by the compound. Traditional filters (Butterworth, Chebyshev, and Bessel) did not work well here as they performed sub-optimally in this respect. Therefore, an implemented bilateral filter was developed here instead of standard 2D/3D filters (23).

Bilateral filter is a 4D Gaussian filter, which works on both spatial and temporal domains, dynamically reserving edges while smoothing the pixels.

In space, the bilateral filter maintains contrast within the images by performing a Gaussian convolution. By judging how different pixel intensities are from the intensity at the center of the user-defined kernel, the 3D filter can replace the center pixel's intensity according to its neighborhood pixels (Figure 3. 2). The spatial bilateral filter was applied here for every frame. Frame means one brain at one time point.
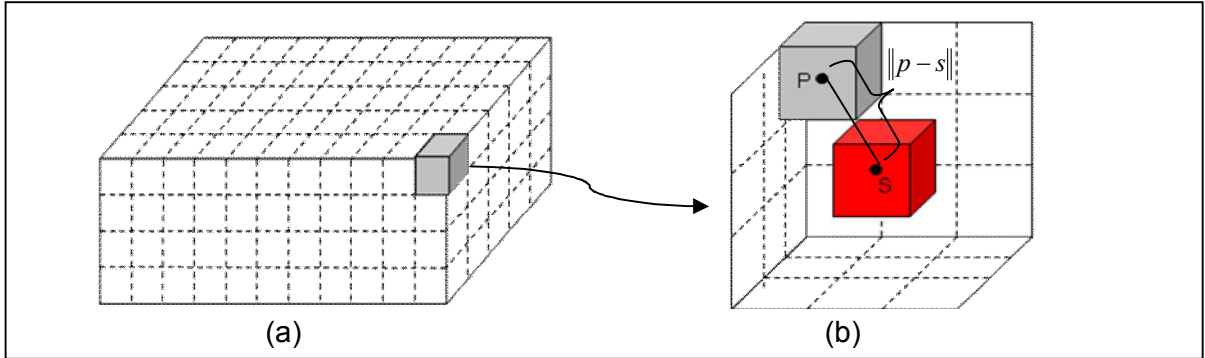
Figure 3. 2 Spatial bilateral filter. (a) One time frame. (b) Neighborhood of voxel s, where p is one voxel within the 3x3x3 kernel.

The formula for the spatial bilateral filter for one pixel s is described below:

$$B(s, \sigma_h, \sigma_i) = \frac{\sum\limits_{p \in N_s} g(\|p - s\|, \sigma_h) g(D(p,s), \sigma_i) I_p}{\sum\limits_{p \in N_s} g(\|p - s\|, \sigma_h) g(D(p,s), \sigma_i)} \; , \qquad [1]$$

$$g(x, \sigma) = e^{\frac{-x^2}{2\sigma^2}} \Big/ (\sigma \sqrt{2\pi}) \; , \qquad [2]$$

$$N_s = \ker nel = \begin{bmatrix} p_x = [s_x - k, s_x + k] \\ p_y = [s_y - k, s_y + k] \end{bmatrix}, \qquad [3]$$

$$D(p,s) = I_p - I_s, \qquad\qquad [4]$$

where B represents the signal intensity of pixel s after spatial bilateral filter, $g(x,\sigma)$ is a Gaussian Filter, N_s stands for the neighbor of central pixel and $D(p,s)$ is the intensity difference between two pixels.

For the temporal part, the idea is to compare local spatial neighborhoods centered at the same pixel in nearby frames (Figure 3. 3). A different similarity distance was used instead of the intensity difference $D(p,s)$ in the spatial filter, since the two pixels' intensity difference cannot provide enough information for judging if they are significantly different.
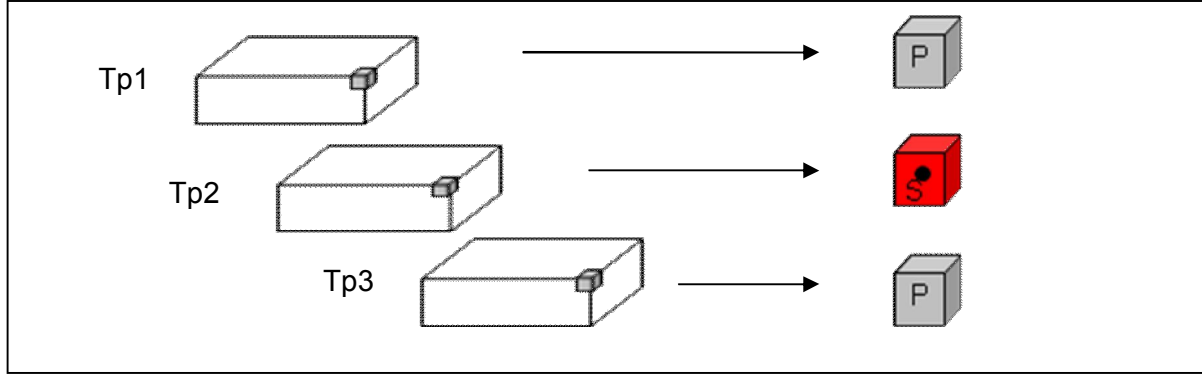
Figure 3. 3 Temporal bilateral filter. Temporal filter is dealing with same voxel neighborhoods within continuous time points.

For comparing two spatial neighborhoods, the following dissimilarity was used.

$$D(p_{xyt}, s_{xyt}) = \frac{\sum\limits_{x=sx-n}^{x=sx+n} \sum\limits_{y=sy-n}^{y=sy+n} g(\|x - p_x, y - p_y\|, \sigma_e) |I_{x,y,pt} - I_{x,y,st}|}{\sum\limits_{x=sx-n}^{x=sx+n} \sum\limits_{y=sy-n}^{y=sy+n} g(\|x - p_x, y - p_y\|, \sigma_e)}, \qquad [5]$$

3.3.1.2 Rigid-body Method

General idea of this method is to find how animal moves by using the SPM motion estimation (24-25) and to compensate the resulting intensity variation accordingly. A reference phantom was used here for computing the intensity correction needed. Figure 3. 4 shows the procedure of the Rigid-body transformation method.

Figure 3. 4 Rigid Body Transformation Method to compensate intensity change caused by motion.

  1) SPM Motion Correction:

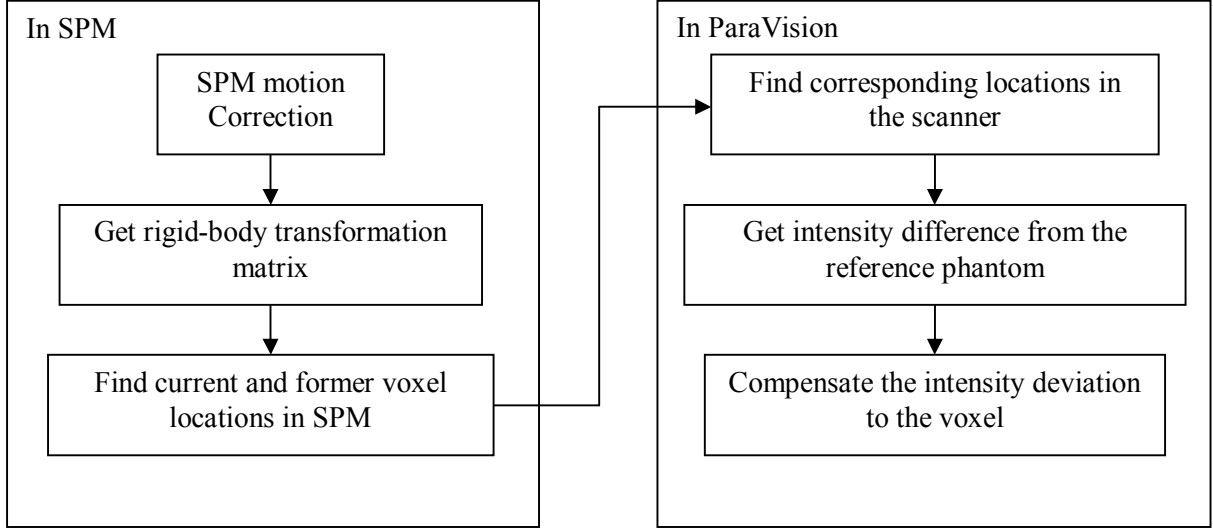In order to make voxels remain the same location in the brain time series during a long scanning, SPM rotates and translates brains according to a reference volume, which is referred to the brain at last scan here. Six parameters are given by motion-correction: 3 translations (x, y, z) and 3 rotations ($pitch, roll, yaw$).

  2) Get Rigid-body Transformation Matrix (26-27):

$$T_t = \begin{pmatrix} 1 & 0 & 0 & x \\ 0 & 1 & 0 & y \\ 0 & 0 & 1 & z \\ 0 & 0 & 0 & 1 \end{pmatrix},$$ [6]

$$T_{rx} = \begin{pmatrix} 1 & 0 & 0 & 0 \\ 0 & \cos(r_x) & \sin(r_x) & 0 \\ 0 & -\sin(r_x) & \cos(r_x) & 0 \\ 0 & 0 & 0 & 1 \end{pmatrix},$$ [7]

$$T_{ry} = \begin{pmatrix} \cos(r_y) & 0 & \sin(r_y) & 0 \\ 0 & 1 & 0 & 0 \\ -\sin(r_y) & 0 & \cos(r_y) & 0 \\ 0 & 0 & 0 & 1 \end{pmatrix},$$ [8]

$$T_{rz} = \begin{pmatrix} \cos(r_z) & \sin(r_z) & 0 & 0 \\ -\sin(r_z) & \cos(r_z) & 0 & 0 \\ 0 & 0 & 1 & 0 \\ 0 & 0 & 0 & 1 \end{pmatrix},$$ [9]

$$T = T_t \cdot T_{rx} \cdot T_{ry} \cdot T_{rz},$$ [10]

11

where x, y, z are the translation parameters, r_x, r_y, r_z stand for pitch, roll and yaw separately, T is the rigid-body transformation matrix.

3) Find Current and Former Voxel Locations in SPM

The current and former voxel locations are found by using the equation:

$$\begin{pmatrix} y_1 \\ y_2 \\ y_3 \\ 1 \end{pmatrix} = T \cdot \begin{pmatrix} x_1 \\ x_2 \\ x_3 \\ 1 \end{pmatrix}, \qquad [11]$$

where (x_1, x_2, x_3) is the original voxel position, (y_1, y_2, y_3) is the voxel position after transformation. Both of the positions are in the SPM coordinate system.

SPM will automatically produce motion-corrected images, in which the coordinate after processing can be found without any problem. Inverse of Eq. [11] can be used for the initial position calculation. Therefore, the positions of one pixel before and after motion-correction can be obtained.

4) Find Corresponding Locations in the Scanner

By locating the voxel positions (original and after motion-correction), the intensity change caused by motion can be estimated from the corresponding positions in the reference phantom. However, brain and phantom images have different resolution, size and position inside the scanner. Thus, for comparing them, a common coordinate system was needed.

ParaVision is the Bruker's industry standard MRI software, which can run a scanner and store all information related to the scan. In ParaVision, there are three different definitions for coordinate systems: patient, user interface and image coordinate system. A data conversion from patient coordinate system into image coordinate system (Figure 3. 5) was required here (28).

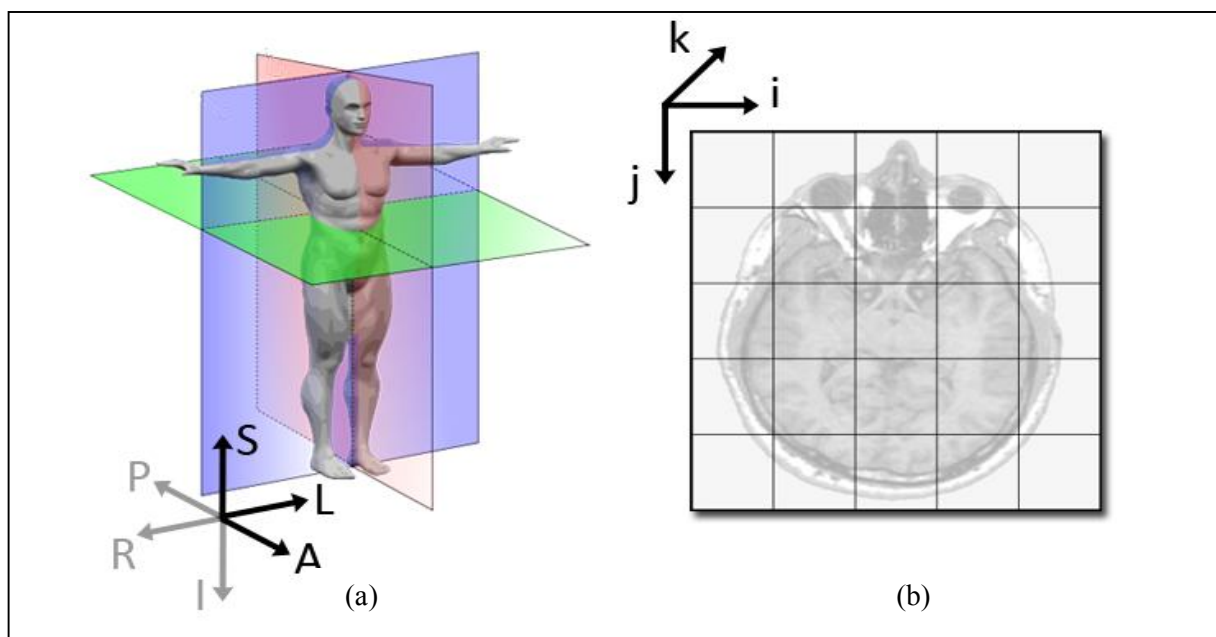**Figure 3. 5 (a) Patient coordinate system (also called anatomical coordinate system). In Neuroimaging, it is common to define the space with respect to the human (animal) whose brain is being scanned. The system will change according to different brain positions. (b) Image coordinate system. It describes how an image was acquired with respect to the anatomy, which will not be affected by subjects' positions.**

In order to transfer data into the image coordinate system, the image description parameters (VisuCore) are important.

The resolution can be calculated by using the equation:

$$r = FOV / s,$$ [12]

Where r is the resolution, FOV is the field of view (VisuCoreExtent) and s is the image size (VisuCoreSize). Both FOV and s are in image coordinate system.

The first voxel position in the image coordinate system can be found by the equation:

$$i = M \cdot p,$$ [13]

where i is the first voxel position in the image coordinate system in mm, M is the orientation matrix (VisuCoreOrientation) and p is the first voxel position (VisuCorePosition) in the patient coordinate system in mm.

Both brain and phantom data were transferred into the image coordinate system (Figure 3. 6). Firstly, the voxel position was converted from pixel position into millimeter based on brain's r and i , and then the voxel position in the phantom in pixel was calculated using phantom's r and i . As shown in Figure 3. 6, it is possible that no corresponding voxel position can be found within the phantom. In that case, the original intensity value will be marked as background. This step is extremely important not only for the rigid-body method but also for the following overlay method.
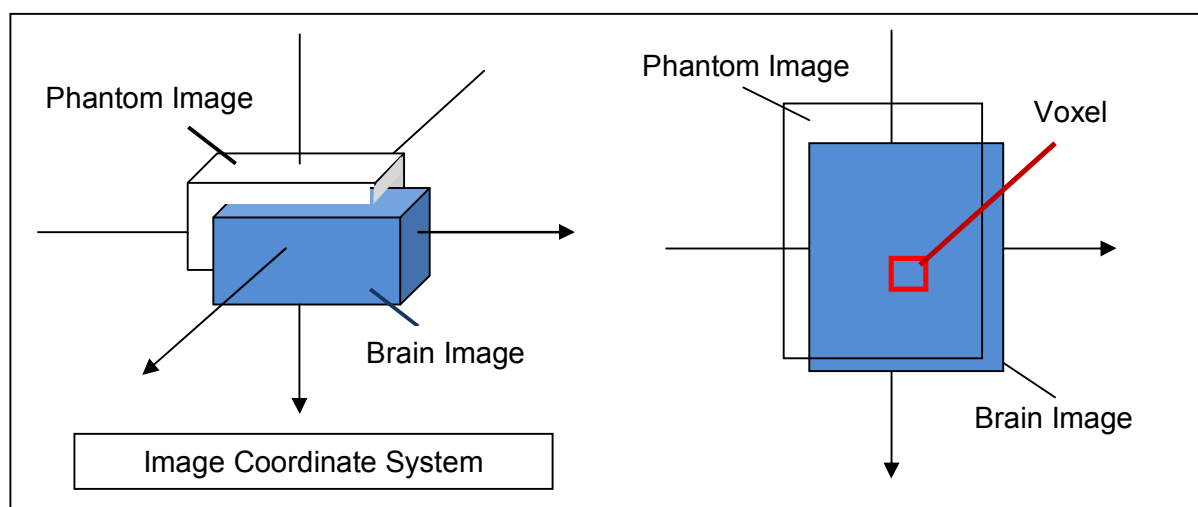
Figure 3. 6 Two objects' spatial position within the image coordinate system.

5) Get intensity Differences from Reference Phantom and Compensate to Brain Voxel Intensity

Since two positions of one voxel (before and after motion correction) can be found in the phantom, the intensities can be read out separately. A ratio between them can be calculated and the brain voxel intensity can be compensated by multiplying the ratio.

$$\frac{I_{Brain\_b}}{I_{Brain\_a}} = \frac{I_{Phantom\_b}}{I_{Phantom\_a}} = c,$$ [14]

Where I_{Brain_b} and I_{Brain_a} represent the brain voxel intensities before and after motion correction,

$I_{Phantom\_b}$ and $I_{Phantom\_a}$ are the phantom voxel intensities of corresponding positions. In Eq. [14], I_{Brain_b}, $I_{Phantom\_b}$ and $I_{Phantom\_a}$ are known in the calculation.

3.3.1.3 Overlay Method

Overlay method also utilizes the uniform reference phantom, but it is more straightforward than the Rigid-body transformation method. The whole procedure of overlay method only works on raw data, which means before the SPM motion correction. The uniform phantom can be considered as a mapping of coil sensitivity and field inhomogeneity. Since the same scan configuration is used on both animal and phantom, they have similar intensity varying trend.
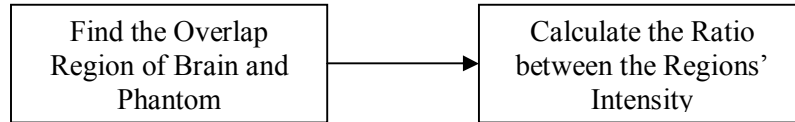
```
┌─────────────────────┐        ┌─────────────────────┐
│  Find the Overlap   │        │  Calculate the Ratio │
│  Region of Brain and│───────▶│  between the Regions'│
│      Phantom        │        │      Intensity       │
└─────────────────────┘        └─────────────────────┘
```

Figure 3. 7 Work frame for overlay method.

The procedure for the overlay method is as follows:

    1)   Find the Overlap Region of Brain and Phantom

The detail for this step is described in 3.1.2 4). Instead of finding a single voxel position, the overlap region of the two objects is used, as shown in Figure 3. 7.

    2)   Calculate the Ratio between the Regions' intensity

$$I_{result} = I_{brain} / I_{phantom} , \qquad\qquad [15]$$

where I_{brain} shows the brain intensity for the overlap region, $I_{phantom}$ represents the phantom intensity for the overlap region. Because of the small value after the division operation, the mean intensity of the phantom is multiplied with the result. Overlay method can eliminate the effect of inhomogeneity signal intensity on voxel's intensity.

3.3.1.4 External Reference Phantom

The thermal drift can be observed in a scanned phantom, so two phantoms were tested here for correcting the signal intensity. However, due to the limitation of space inside the scanner, silicon phantom which was injected in animal ear was selected.

  With the assumption that, the phantom signal intensity and T_2* are constant when there is no thermal variation, a matrix for correction can be obtained.

  First, phantom signal intensities of all time points were averaged at each echo. These mean values were considered as the reference signal intensities at a constant temperature. Second, the ratio between the mean value and intensities at the same echo were calculated. Thus the correction matrix was generated, which was then multiplied by all the pixels in animal brain area to remove thermal effect.

  The equation to calculate correction-matrix:

$$\begin{pmatrix} S_{1\_mean} \\ S_{2\_mean} \\ S_{3\_mean} \\ \vdots \\ S_{n\_mean} \end{pmatrix} = M \cdot \begin{pmatrix} S_1 \\ S_2 \\ S_3 \\ \vdots \\ S_n \end{pmatrix}, \qquad [16]$$

where $S_1 \dots S_n$ are averaged intensities in phantom area of all time points at each echo (echo number= n). $S_{1\_mean} \dots S_{n\_mean}$ are the mean values of $S_1 \dots S_n$. M is the correction matrix. The matrix represents thermal drift factors at all echoes over time, which has the same size as signal intensities of one pixel. So it is easy to correct brain signals by simply multiplying the matrix.

3.3.2 SPM Spatial Processing

SPM effectively processes image data to remove motion, and normalizes data acquired from different animals to the same animal template for the statistical analysis. Schematic of SPM spatial processing (24-25) is displayed in Figure 3. 8Figure 3. 8 (a) Schematic of SPM spatial processing. (b) Important parameters for 6-parameter rigid-body transformation.. Three steps are included:
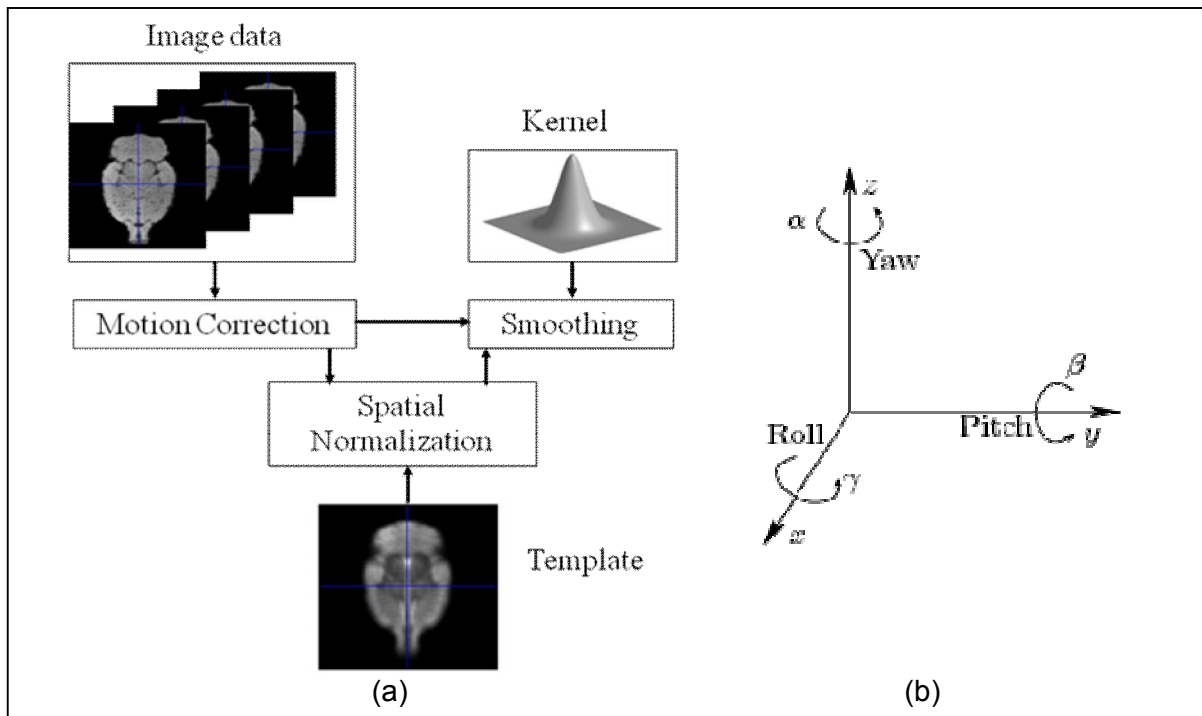

(a)   (b)

Figure 3. 8 (a) Schematic of SPM spatial processing. (b) Important parameters for 6-parameter rigid-body transformation.

1) Motion correction

Motion correction is known as realignment in SPM, and it aims to remove movement artifact a time series. Realignment is calculated by using a least squares approach and a six-parameter spatial transformation, which realigns a time-series of images from the same subject to single reference time frame.

2) Normalization

In order to compare data from several scans or subjects, all the brain images need to be normalized in the same 3D space. Normalization warps motion-corrected images to fit to a standard template brain

(Here, an average of several rats brain dataset) and reduces potentially large differences in size and structure among the brain images of subjects, improving the power of statistical analysis and enabling group-level comparisons.

3) Smoothing

By applying a spatial filtering with appropriate kernel size ($1x1x1mm^3$ in our study), signal to noise ratio will be increased. Also, motion-correction and normalization algorithm can generate Not-A-Number (NaN) pixels in the image data, which makes statistical analysis invalid. Spatial smoothing can eliminate these insignificant values as well.

3.3.3 T_2* Maps

Except signal intensity, another MRI parameter named T_2*, and its inverse R_2* were used for analysis for dataset B. T_2* is a transverse relaxation time constant, which reveals tissue property. Compared to signal intensity, the advantage of T_2* is that its change is linearly related to the rCBV change, which will be discussed in the last part of this chapter.

After SPM spatial processing, statistical analysis will be performed to the T_2*-weighted data of dataset A, while for the dataset B, T_2*/R_2* maps were obtained before further processing.

T_2*/R_2* calculation:

Gradient echo signal intensities decay over echo time. From multi-echo gradient echo images, T_2* can be calculated by a mono-exponential fitting Eq. [17]:

$$S = a \cdot e^{-bTE}, \qquad [17]$$

where S is the signal intensity over echo-time series. The component b equals R_2*, TE is the echoes in millisecond and a is a constant.

The parameter b is calculated by using the equation:

$$b = \frac{\sum_i \sum_j S_i S_j \left[\ln S_i - \ln S_j\right][i-j]}{\Delta TE \sum_i \sum_j S_i S_j [i-j]^2}, \qquad [18]$$

where i and j are echo numbers, S_i and S_j are signal intensity at echo i and j respectively. And ΔTE is the echo interval (in milliseconds).

T_2* maps were then analyzed statistically to find out the brain activation map. R_2* maps were also calculated by inversing the T_2* maps, and a mask was used to exclude the pixels outside the brain.

3.4 Data Analysis

Statistical data analysis can be divided into two parts: location of the activated brain regions and quantification of the compound effect.

3.4.1 Location of the Activated Regions

In order to locate the significant response regions, two groups are required — vehicle and treated groups. The time-intensity/T_2* curve of one pixel in a vehicle animal after CA administration rises over time as the CA concentration is reducing. The curve is called a clearance curve, which represents the animal's ability to remove the CA from the blood circulation. All tissues in one animal have same clearance rate, but when measured by MRI, the rates are different between individual voxels. One reason is that large blood vessels strongly affect the signal intensity in its surrounding, which is quite different from capillaries. And each animal has its own clearance rate as well.

Treated group always has injections twice, one with contrast agent and the other with compound. The time-intensity curve of a treated group actually equals to two effects' combination. Vehicle group animals receive the same treatment procedure as the treated group except using vehicle solution rather than the compound administration. To figure out how the compound affects, the clearance curve introduced by contrast agent should be eliminated.

Based on the theory above, three different analysis approaches were developed here in our work:

3.4.1.1 Time-bin Method

SPM statistical analysis (29-30) uses General Linear Model (GLM) to describe the data instability in terms of noise, experimental effects, and residual variation. According to different usages, SPM analysis is separated into two steps.

First-level analysis: A within-subject analysis, which deals with all the subjects separately. First-level analysis is a preparation for the group comparison, and is used to produce appropriate summary data.

The main functions of the first analysis are:
   I.   Specify GLM design matrix, dataset and processing methods.
   II.   Estimate GLM parameters using classical or Bayesian approaches.

$$y = X \cdot \beta + E, \qquad\qquad [19]$$

where y is the original curve, X is the design matrix, β represents the estimated parameters and E is the residual noise or error.

The design matrix (regressor) has one row for each scan and one column for each explanatory. Our design matrix was defined manually to follow the Time-bin order. For compound A, the design matrix had 5 columns standing for 5 betas, and 38 rows representing 38 time points. While for compound B, the regressor was selected as 5 columns to subsequently represent time points 15 to 80. Betas are the parameters of concern, which are used in 'second-level analysis'. In essence, betas are the slopes at time intervals defined by the regressor (Figure 3. 9).
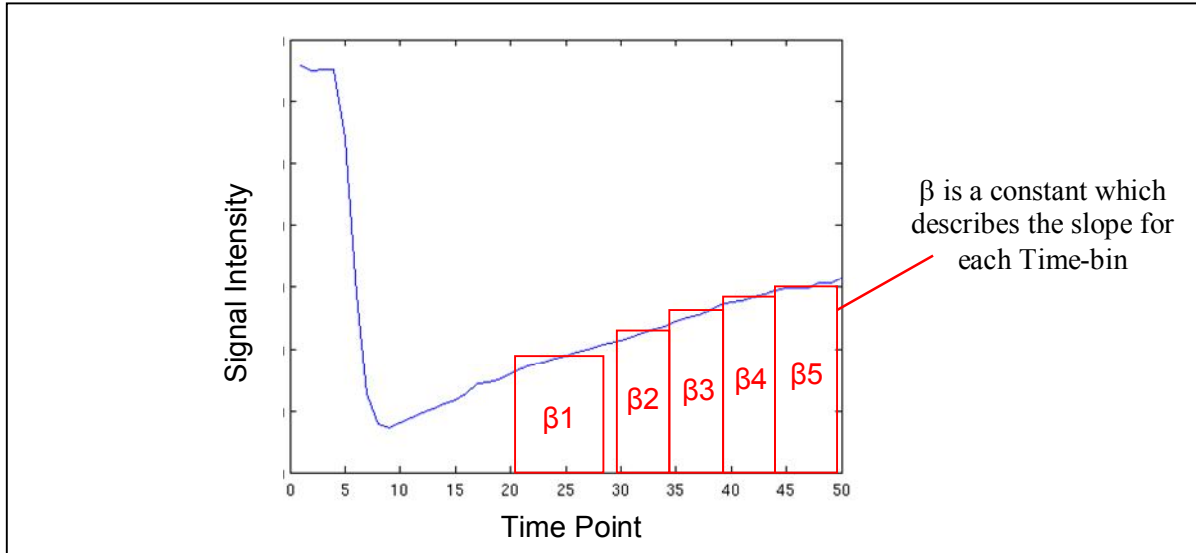
Figure 3. 9 First level analysis: design matrix (regressor) and beta.

Second-level analysis: A multi-subject statistical analysis, which is used for testing the difference between two groups. In the second-level analysis, beta images from first-level analysis were used for comparison between groups. But different from the design matrix in first-level analysis, the rows represent subjects or between-subject variability; columns represent the specified effects of interest.

Once the result model was generated, by selecting a proper contrast, the activation map can be checked.

For A dataset, subjects from vehicle group and three treated groups (0.9mM, 4.8mM and 28mM) were analyzed by SPM first and second level analysis. Similarly, subjects from vehicle and substance group for compound B were analyzed. One disadvantage of this method is the low sensitivity and accuracy, which inspired a more advanced approach in this session (3.1.4.3).

3.4.1.2 Shuffle Method

Shuffle method is a development of SPM second-level analysis. In the output of SPM statistic analysis, there are t-contrasts and F-contrasts results in GLM. Our interest is in one of the t-contrasts results— Positive effects of Group_1, showing regions with significantly positive effect between two groups.

t-contrasts results are calculated by using t-test. A t-test can be any statistical hypothesis test which follows the student t-distribution.

Probability density function:

$$f(t) = \frac{1}{\sqrt{v}B(\frac{1}{2}, \frac{v}{2})} \cdot (1 + \frac{t^2}{v})^{-\frac{v+1}{2}} ,$$
[20]

where v is the degree of freedom, B is the Beta function. The student t-distribution curve is shown in Figure 3.10.

Another important parameter which needs to be referred here is called the p-value. In a statistical significance test, the p-value is the probability of uncertainty which is used to measure if an effect is significant or not. When the p-value is lower than the significance level (normally 0.05 or 0.1), it is called 'reject the null hypothesis'. Once the null hypothesis is rejected, the result is considered to be statistically significant.
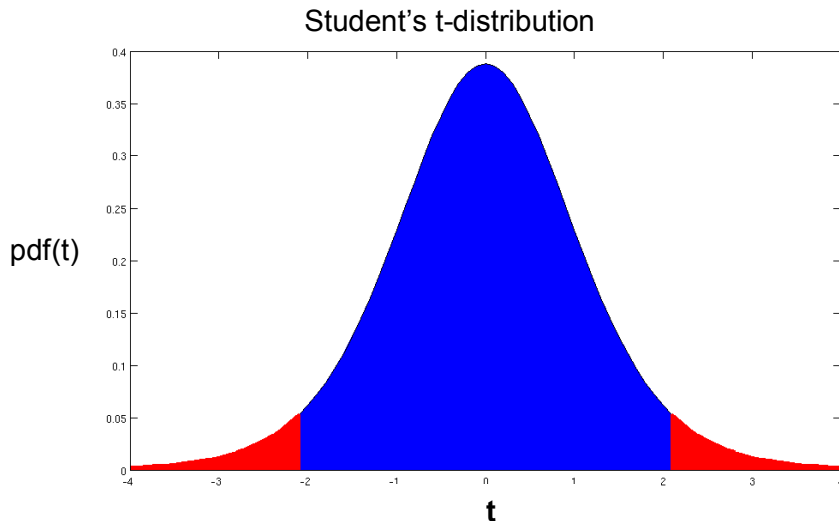
Figure 3. 10 Generate p-value from t-distribution

Figure 3.10 shows the theoretical relationship between t-test and p-value:

$$p = red\_area / (red\_area + blue\_area) \qquad\qquad [21]$$

Here the x label is t-value, and y label is probability distribution function of t-value. To simplify the problem, in our calculation, y-label was the number of votes for each t. Meanwhile, here p represents the probability that absolute t-value above a certain threshold.

However, in reality, the T values may not always follow the ideal Student's-distribution (Figure 3. 10). Therefore, shuffle method was used here to get the real distribution.
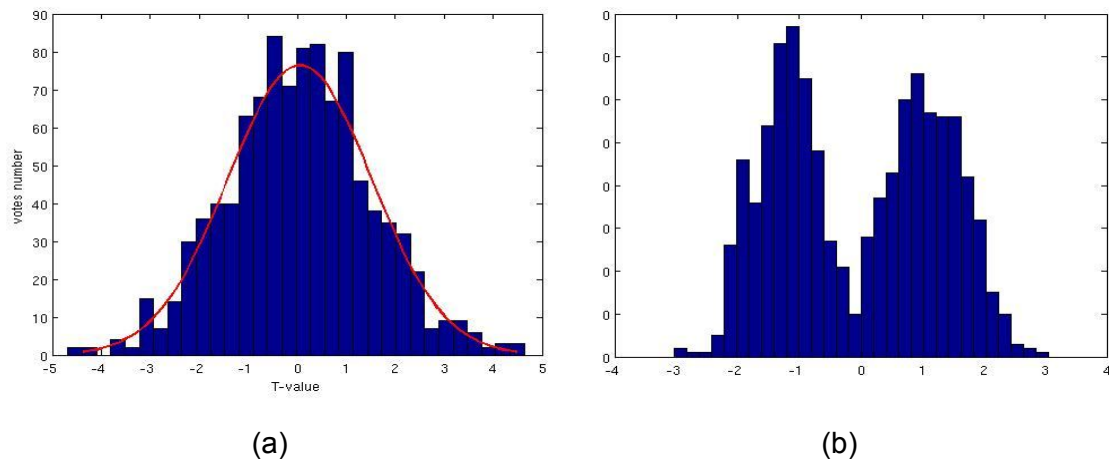

(a)   (b)

Figure 3. 11 T-distribution of two randomly selected pixels after reshuffle. (a) T-distribution of one pixel. (b) T-distribution of the other pixel

Figure 3.11 displays the t-distributions for two pixels; which obviously are of different shapes. It can prove that in reality not all pixels' histograms follow the student's t-distribution.
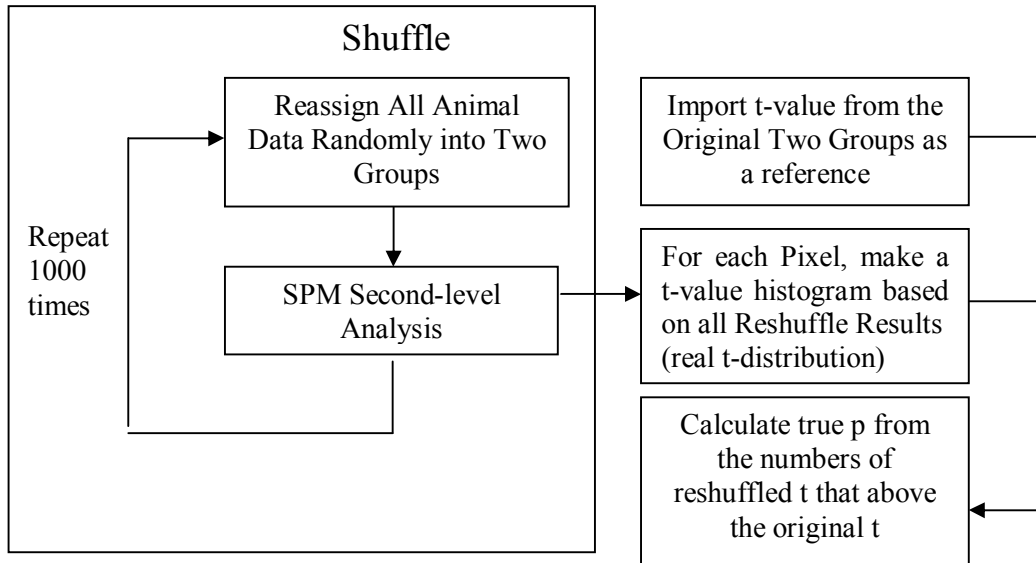
19

Figure 3. 12 Work frame of the shuffle method to get the real p-value. The animal data were randomly divided into two groups and analyzed by SPM. After repeat this process for 1000 times (shuffle), these results (real t-distribution) from SPM were used to calculate true p values for each pixel.

After thousand times reshuffle and reanalysis, 1000 T-values were calculated for each pixel. The true p-value was generated from the probability of the extreme T-values. In order to get the true p-value, a proper threshold for t-distribution should be chosen for every pixel. The original T-values from two groups were used as a reference threshold for the real t-distribution, and the probability of the absolute T-values above the threshold was the real p.

3.4.1.3 Clearance Model Method

Idea of this method is to find the clearance curve for each animal and remove it from the time curve. Clearance curve here is a curve which only contains the effect of contrast agent and vehicle solution over time. After eliminating it from the raw curve, what are left will be the compound effect and its region distribution and magnitude can be quantified. However, the variation caused by compound is much smaller compared to that caused by contrast agent. Animals have different clearance rates as well, thus the clearance curve of a vehicle group cannot accurately represent that of the treated animals.

   To describe the real clearance curve for all the animals, functional and numerical methods are explained below:

   I.   Clearance Model

1) Functional Method:
Theoretically, the clearance curve can be described by the equation:

$$Y = A \cdot e^{C*t} + B \qquad\qquad [22]$$

where Y can be either signal intensity or T2*, A is a constant, C is the clearance rate, representing functionality of animal to clear contrast agent, t is time, and B is a constant.

   Functional method uses a least-square approach to fit the Eq. [21] to all animals' time-intensity/time-T_2* curves. The resulting 'fitted brains' were named 'sample group', and used as the animals' clearance curves instead of vehicle group animals. Finding the difference between original and fitted brains, the real activated regions should be found where the difference is larger. But Vehicle

group turns to be useless in this view. For vehicle animals, all the time points after CA injection can be counted into the calculation, which bring us really good fitting. Yet for treated group, only pre-substance period can be used for computation, and the time points after that have to be extrapolated.

2) Numerical method:

An improvement to the functional method is to produce a numerical clearance model instead of functional curve fitting. Numerical model is based on vehicle data, where the procedure is shown below:
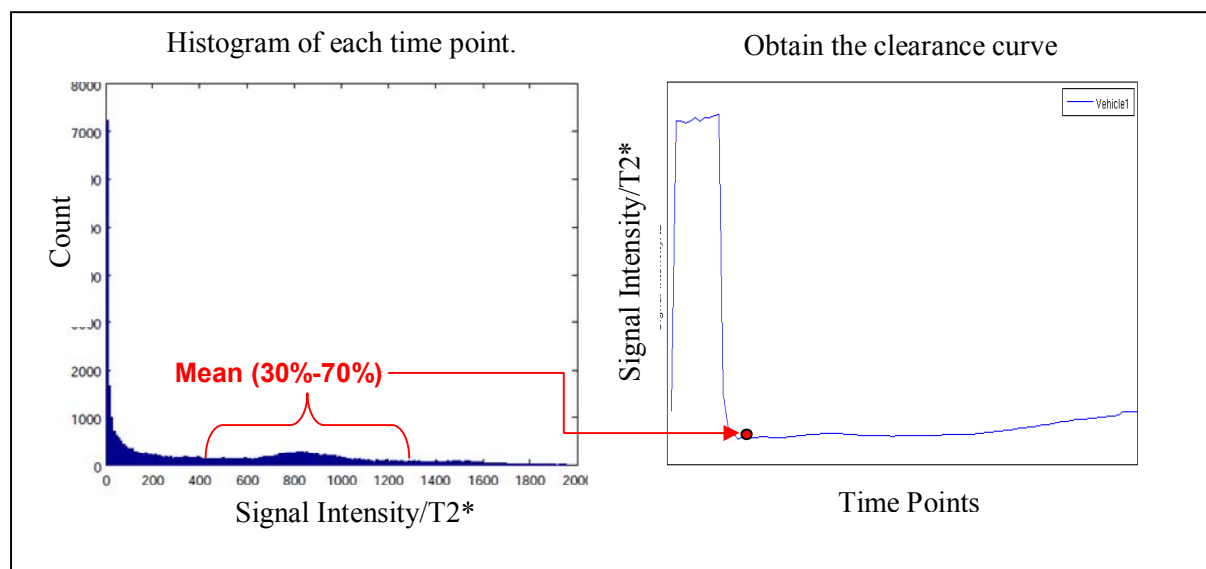
    a) Obtain the clearance curve for each vehicle animal

Figure 3. 13 The way to get clearance curve from mean vehicle animals.

By selecting one animal dataset from vehicle group, the signal intensity/T_2* histogram at each time point was obtained. In order to exclude all the extreme values and average the remains, the mean of 30% to 70% of the whole histogram was calculated. The resulting value can stand for the global intensity/T_2* value at the certain time point. The procedure repeats for all the time points, resulting in a clearance curve which can represent the effect by contrast agent and vehicle solution for this animal.

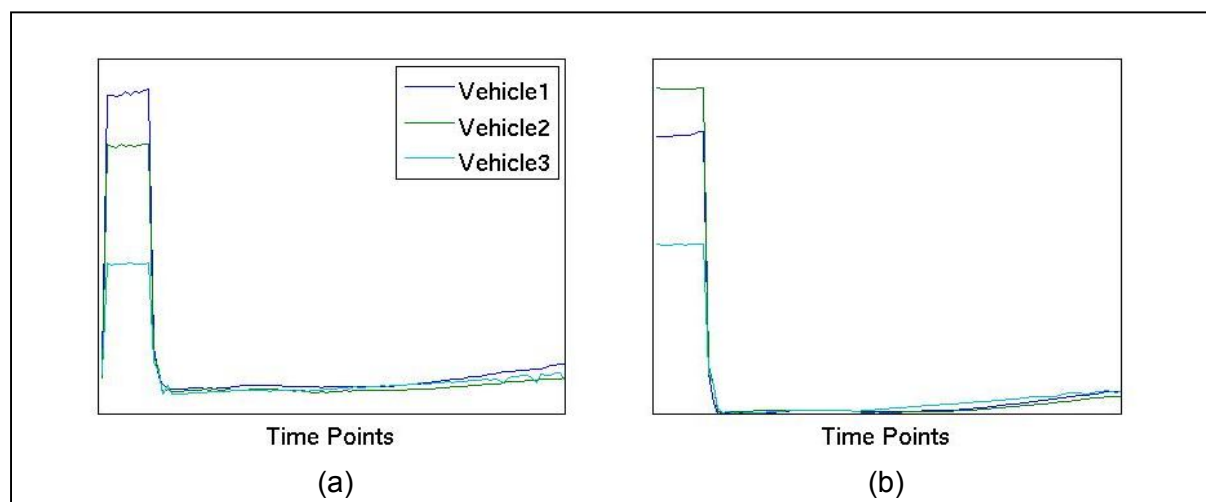   b) Normalize clearance curves of all the vehicle animals

Figure 3. 14 Rescale all the curves of vehicle animals. (a) Before rescaling. (b) After rescaling.

Clearance curve of each animal in vehicle group can be obtained in step I (Figure 3. 14 (a)). They have a similar pattern but different initial value and scaling. To normalize all the curves, their individual offsets were removed. The smallest value is regarded as the end of CA administration. The whole curve after the CA administration is the pure clearance curve. Normalize all the clearance curves and ensure them go through same value at the last time point before substance administration (Figure 3. 14 (b)).

  c) Obtain a general clearance model of vehicle group

After all the clearance curves from vehicle animals were normalized, the general clearance model can be acquired by simply averaging all the curves. Hence, the numerical clearance curve represents the general behavior of how fast the contrast agent is removed by the blood circulation.

  The vehicle animal information and the clearance curve should be fitted to each compound animal. One thing to mention is that, it should be adjusted individually to each animal as the individual clearing rates are different. Therefore, for each pixel, the clearance model is fitted during the period of contrast agent but before the substance admitted with least square errors, and is extrapolated in the rest of the time points (Figure 3. 15 (c)). This is because contrast agent is given both in vehicle and compound animals, fitting of that part should be optimized, and with the extrapolation at further time points, the difference between pixel's time curve and clearance model can appear, which can be a compound effect.
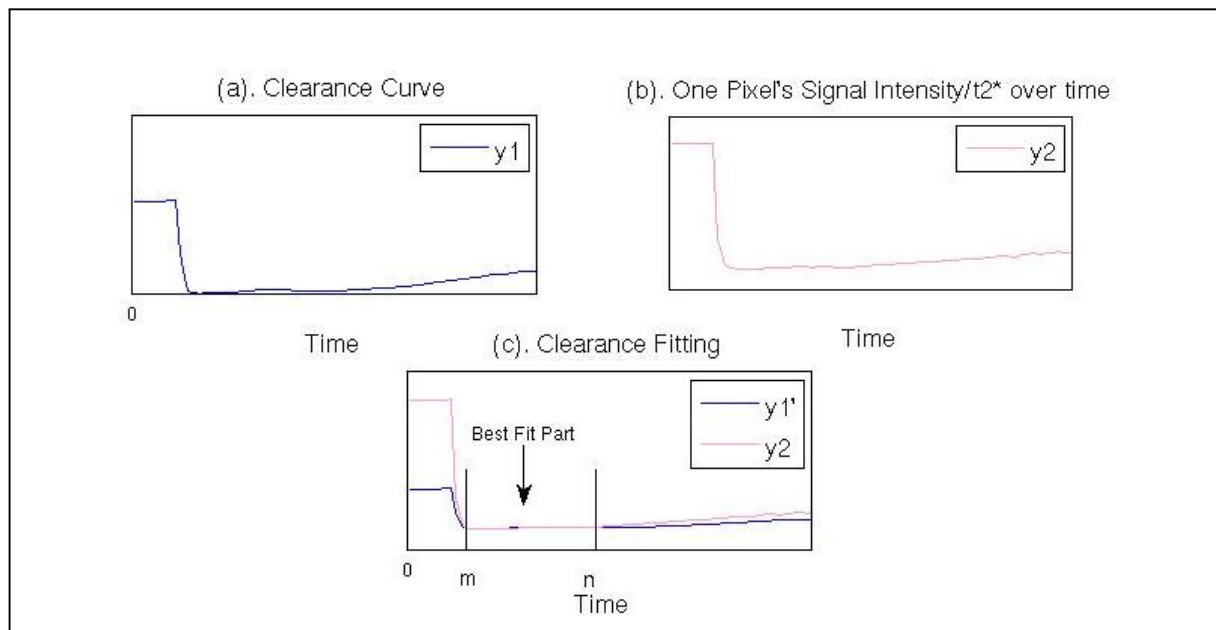

Figure 3. 15 Schematic representation of the clearance model formation. (a) Once the clearance model have been built, (b) every pixel in the brain has its own time curve. (c) Time point m is the time point when the contrast agent is fully injected, and Time point n is when substance is injected. Clearance model is linearly fitted with least square error in this time range, and extrapolate after the time point n.

With least square error method, coefficient a and b are determined so that the clearance model can best fit the pixel's time curve from the time point m to n (Eq. [22]). These two coefficients are applied for the whole clearance model (Eq. [23]), generating a tailored clearance for this pixel.

$$y2 = a \cdot y1 + b, m < Tp < n \qquad [23]$$
$$y1' = a \cdot y1 + b, 0 < Tp < Tp\_end \qquad [24]$$

After the clearance model has been built, it will be fitted for all individual pixels in the compound animal dataset. For individual animal, this pattern should be linearly fitted to suit that animal's

property. And the fitted clearance curve ($y1'$) is taken as the vehicle curve of the compound animal. Therefore, for each compound animal, there generated its own clearance-curve-fitted dataset, which can be taken as its own vehicle animal.

Hence, datasets that can be used in SPM analysis were: original vehicle and compound group, the clearance-curve-fitted group ($y1'$), which we call it sample group. Two statistical approaches to analyze the data were implemented: Time-bin method and clearance curve extraction.

      II.   Clearance curve matching and Time-bin method

After matching clearance model to all the treated animals, the Time-bin method based on SPM can be applied again. Instead of comparing vehicle and treated groups, the matched clearance curves were considered as a sample group which was used to analyze with the treated groups.

      III.   Clearance curve matching and extraction

This is another method applied for dataset A based on clearance model method. That method used the whole fitted curve as the sample group, which may introduce some artifacts according to the inaccuracy of curve fitting, especially in later time points. For getting higher sensitivity, here the early time points of the fitted curve were used to do a one sample t-test manually.

1) For the time points 21 to 30, mean value of the difference between the original and the sample brains for each treated animal was calculated.
2) Perform one sample t-test to each pixel of all the treated animals.

One-sample t-test performs a t-test with the null hypothesis that data come from a normal distribution with mean 0 against the alternative that the mean is not 0. For one pixel, if the mean-differences histogram follows a standard normal distribution, it is considered to be no response. In practice, a rejection of null hypothesis is shown at the 5% significance level.

3.4.2 Quantification — ΔrCBV Calculation

ΔrCBV calculation requires data from vehicle and compound groups, which also used the sample group as vehicle data. Here, the clearance model was used to fit the curves of different treated groups instead of individual animals. The time course in each pixel is an average of all animals' data in that group.

For signal intensity, ΔrCBV can be calculated as (Eq. [24]):

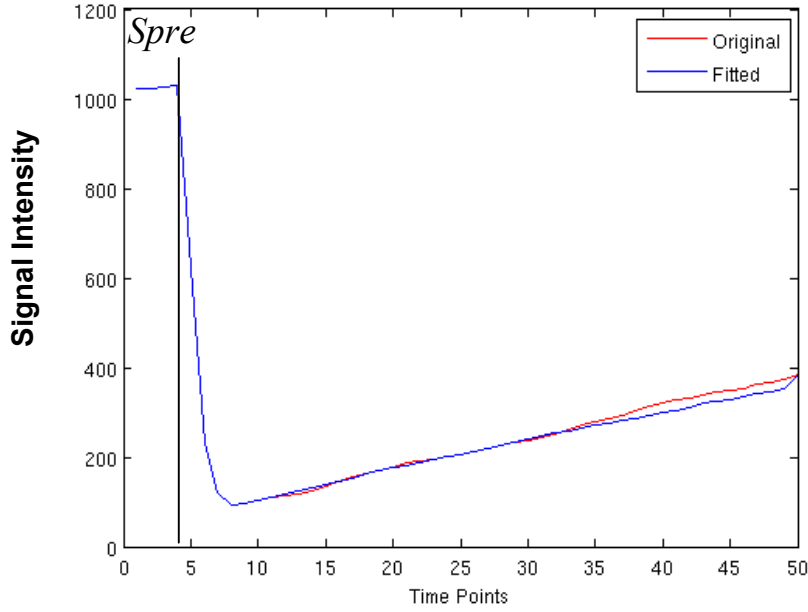$$\Delta rCBV = \{\ln[S(t)/B(t)]\}/\{\ln[B(t)/Spre]\}, \qquad\qquad [25]$$

Figure 3. 16 ΔrCBV calculation from the signal intensity

where $S(t)$ is the original intensity curve for one pixel in a mean treated brain. And $B(t)$ is the fitted clearance curve for one pixel in a mean treated brain. $Spre$ equals mean value of the baseline (Figure 3. 16).

For the R2*-based ΔrCBV calculation (Eq. [26]):

$$\Delta rCBV = k \cdot \left(CBV_{post} - CBV_{pre} \right) = b = b_{post} - b_{pre},$$ [26]
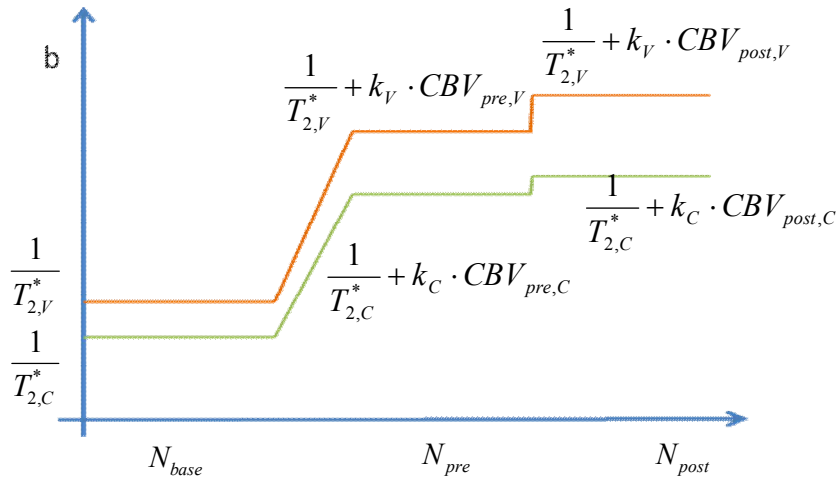

Figure 3. 17 ΔrCBV calculation by R$_2$*

where b is R_2*, k_V, k_C are vehicle and compound group's functions of the contrast agent's concentration in blood and its effect to the surrounding tissue's R_2*.

$\dfrac{1}{T_{2,V}^*}$ and $\dfrac{1}{T_{2,C}^*}$ are the inverse of T2* of vehicle and compound group respectively.

N_{base}, N_{pre}, N_{post} are the time periods for baseline, pre-substance (contrast agent), and post-substance.

Non-zero ΔrCBV can be interpreted as drug-induced activation. The higher the value is, the stronger the brain response to the compound.

For compound A, curve-fitted data as clearance curve (B(t)), and three compound groups, 0.9 mM, 4.8mM and 28mM groups (S(t)) were used to calculate ΔrCBV. Three different results at three concentrations were calculated.

For compound B, the data consists of only one concentration of substance, ΔrCBV was used to verify the activation map generated by SPM.

Chapter 4 **Results**

4.1 Intensity Correction

4.1.1 Bilateral Filter

The four dimensional bilateral filter was employed on each brain volume with a three dimensional kernel size of 5x5x3 pixels. Figure 4. 1(a) shows the 3-D smoothing of one randomly selected pixel's intensity time course of eight echoes in dataset B. As the kernel covers a wide neighborhood, the center pixel's signal intensity is modulated by other pixels inside kernel, especially the intensity curve at echoes five and seven. After that the smoothing on the fourth dimension, with the temporal kernel size of 5 was performed. Figure (b) shows the comparison of one pixel's time-intensity curve before and after 4-D bilateral filter processing. The curve is relatively smooth after the time point 10.

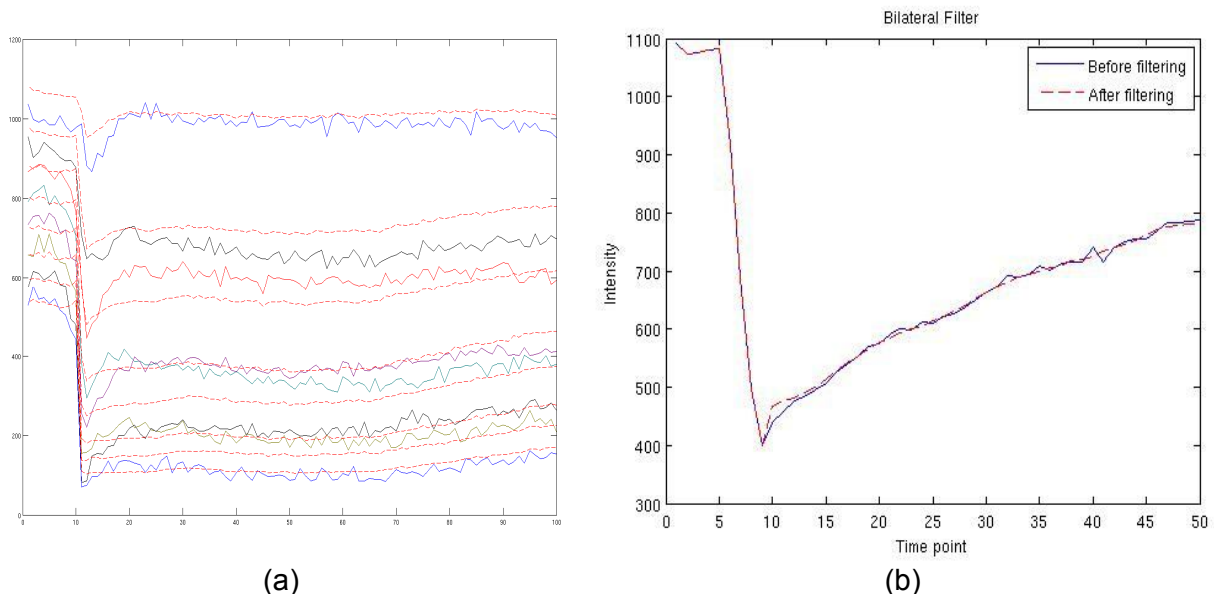(a)   (b)

Figure 4. 1 4-D bilateral filter, (a) 3-D smoothing of one pixel's intensity curve in dataset B (raw data of 8 echoes, and filtered data in red dots), (b) 4-D smoothing of one pixel's intensity curve in dataset A.

After filtering all the vehicle and compound animals' data in dataset A, the statistical analysis to find the group difference was performed between them. The resulting activations are highly unsymmetrical and the p-value is high as well, indicating that there is a high probability that these activations are not real (Figure 4. 2).
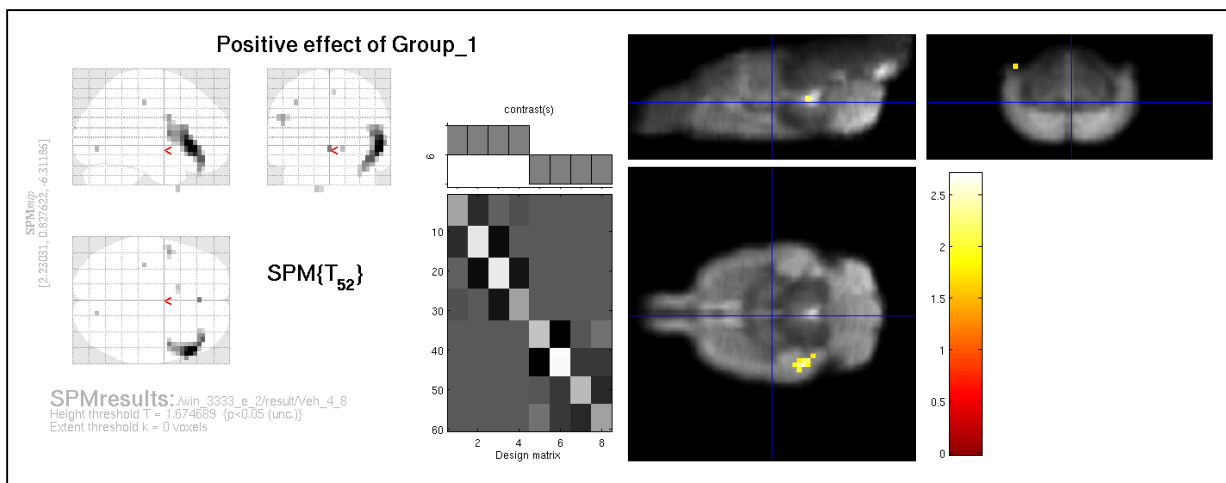

Figure 4. 2 Activation map of dataset A by SPM group analysis on 4-D bilateral filtered vehicle and compound group. Colored regions on the right show regions which were significantly different (p<0.05, unc).

4.1.2 Rigid-body Method Result

As described in 3.1.2, rigid-body transformation method can be divided into two parts: SPM and ParaVision parts. SPM part was used for finding voxel positions before and after SPM motion correction by using rigid-body transformation. ParaVision part attempted to find the intensity differences between corresponding positions in the uniform reference phantom and compensate the signal intensity variation back to the brain images.
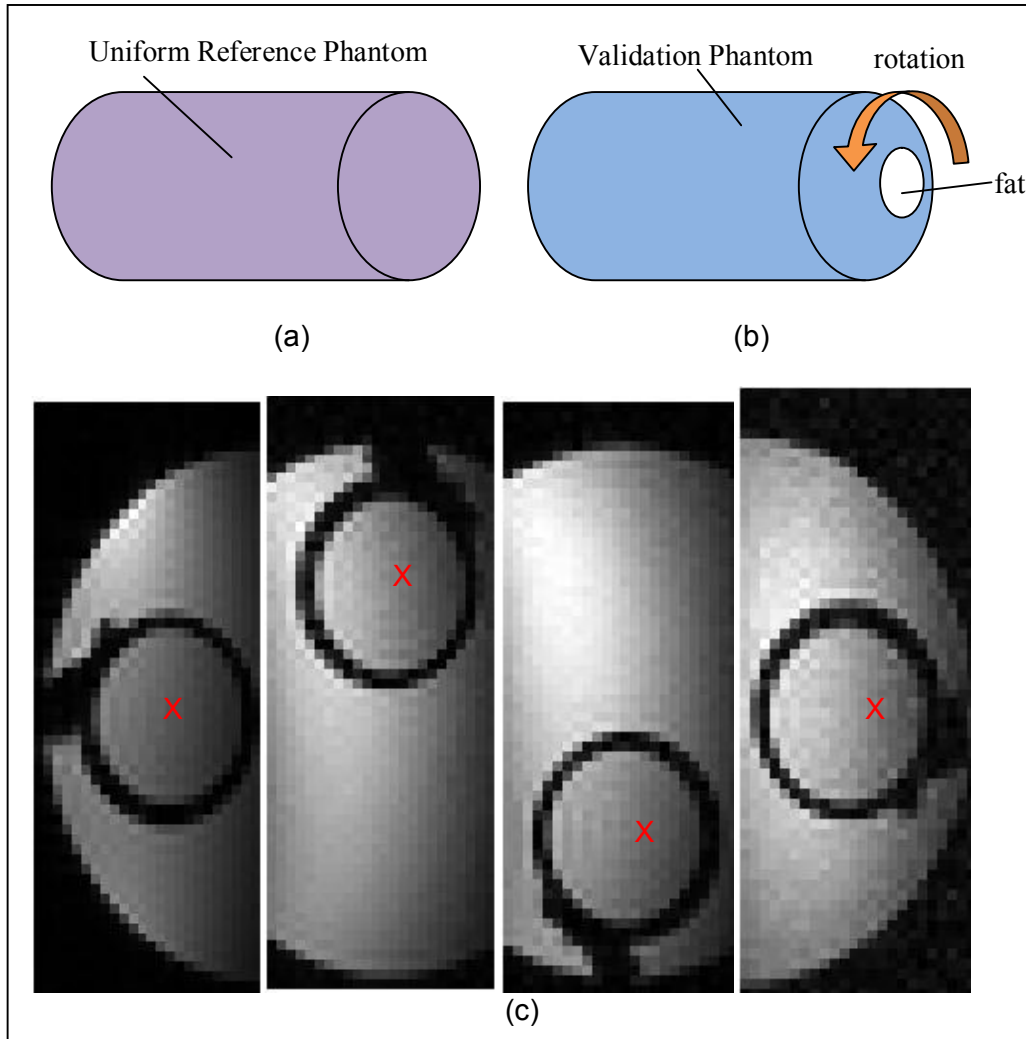

Figure 4. 3 The setup to validate the rigid body transformation algorithm. (a) A uniform reference phantom filled with water was used as a reference. (b) The validation phantom which had a smaller cylinder filled with oil inside was rotated in the scanner. (c) Rotation of 90 degrees was repeated three times, and the position of one pixel (red cross) was identified and followed, and its signal intensities were observed before and after the correction.

This experiment simulated animals' head motion. In the raw validation phantom, one pixel inside fat of the first image is selected, labeled with a red-cross. And other three positions were located by calculation, ensuring that the four crosses represent the same pixel which moves with phantom rotation inside the scanner. After the correction in ParaVision part, the intensities of the four locations should be the same after compensating the intensity differences. Figure 4. 4 shows the measured signal intensities before and after the intensity compensation. Signal intensities greatly vary according to the blue line. It is easy to notice that signal intensity after correction is more equal than the original, which means the compensation method is reasonable if we find the correct spatial locations.
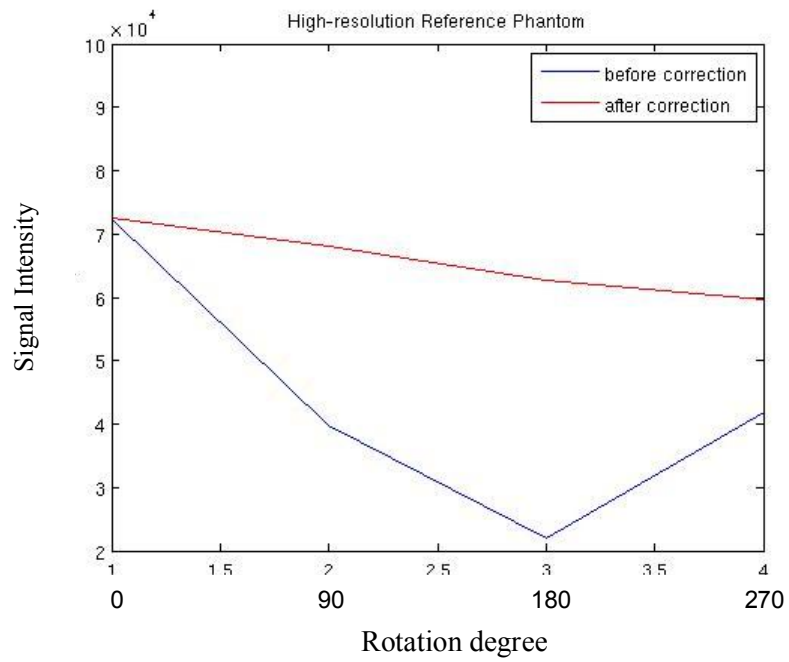
Figure 4. 4 Signal intensities before and after intensity compensation for the crosses pixels in the validation phantom.

It also can be seen from Figure 4. 4 that the signal intensity after compensation was not perfect. The possible reason is that scan configurations of acquiring the four images are not totally the same: a partial field of view was scanned instead of the whole validation phantom, and ParaVision automatically rescales the image signal intensities for each scan.

4.1.3 Overlay Method

The overlay method was tested by acquiring a set of routed image from the validation phantom (size=128x64x24) and one axial slice from the uniform reference phantom (size=128x64x55) using the same surface array coil as a receiver Figure 4. 5. The overlay algorithm was then applied to the validation phantom images to correct the signal intensity variations.
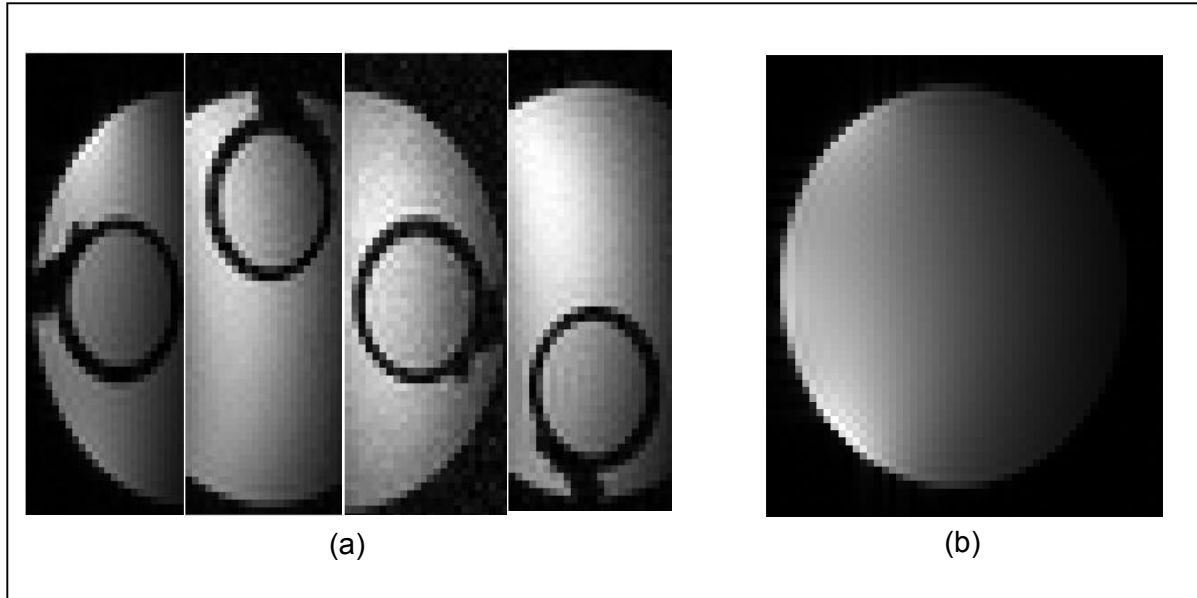

Figure 4. 5 (a) Four scan images from the validation phantom, and (b) is one axial slice of the uniform reference phantom. The idea is to find corresponding spatial regions in (b).

Figure 4. 6 shows the result of the validation phantom test by using overlay method. The algorithm was able to find the spatially corresponding pixels in the validation and the reference phantoms. Also, the signal intensity after the overlay operation is substantially, but not perfectly homogeneous. The imperfect results were caused by same reasons as mentioned in the previous page. In order to acquire the validation phantom data, rotation and reconfiguration of the scan region were necessary, which result in the intensity rescale of ParaVision.
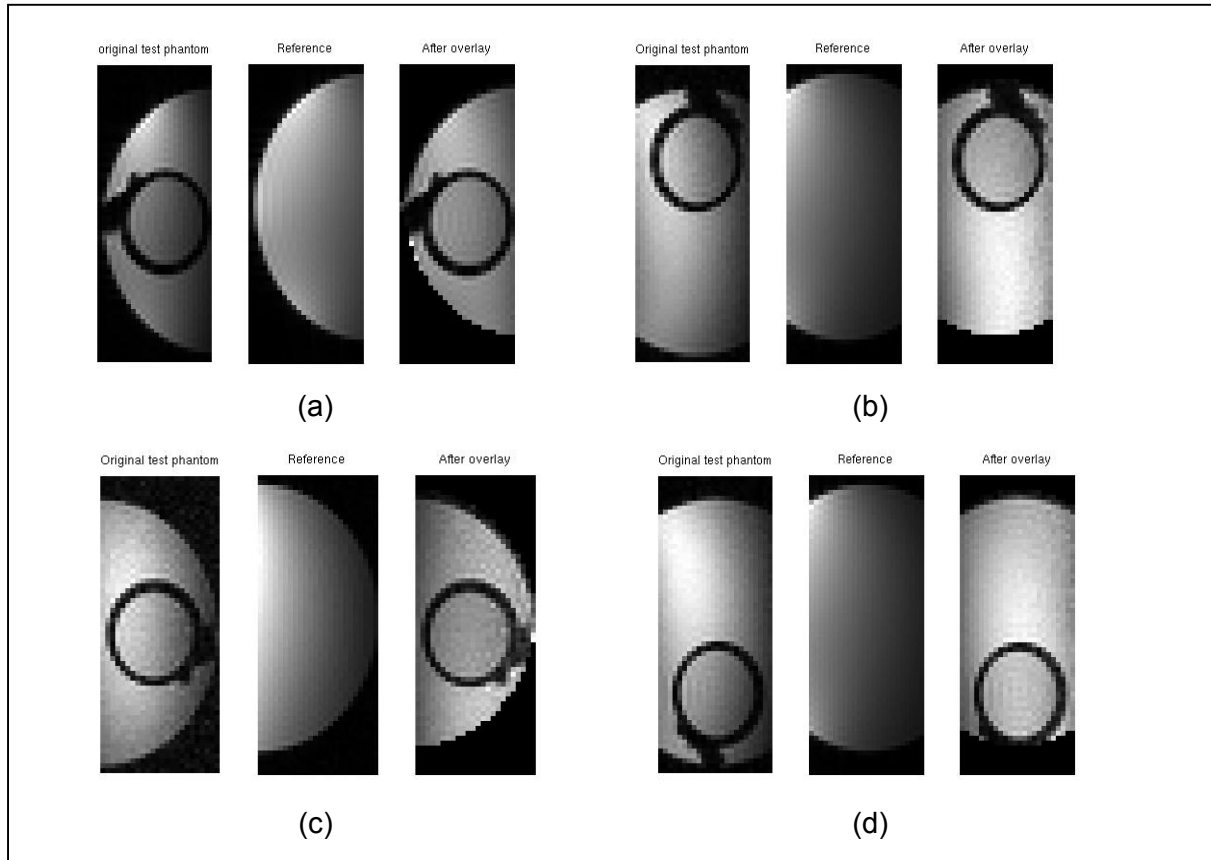
Figure 4. 6 Result of the overlay method on the phantom data. In the left of the images (a-d) are the axial views of the validation phantom where the images have been acquired as four different rotation positions with respect of the receiver coil. In the right are the same images after the overlay correction. In the middle are the corresponding slices of the uniform reference phantom

In Figure 4. 7, the overlay approach has been applied on the raw brain image data. It can be seen that signal intensities in low signal regions become brighter, and the contrast in the image is generally improved.
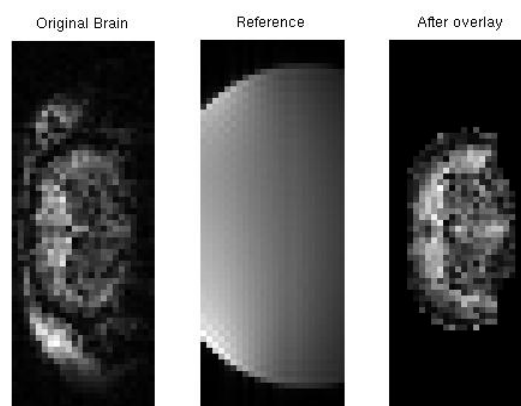

Figure 4. 7 Result of the overlay method on a raw brain image data. Left: original brain image. Middle: corresponding reference phantom. Right: intensity corrected brain image.

According to the Figure 3. 6, the reference phantom has to be large enough to cover all the possible brain positions. No matter how the animal moves within the scanner, overlay algorithm can always find a corresponding overlap region from the uniform reference phantom.
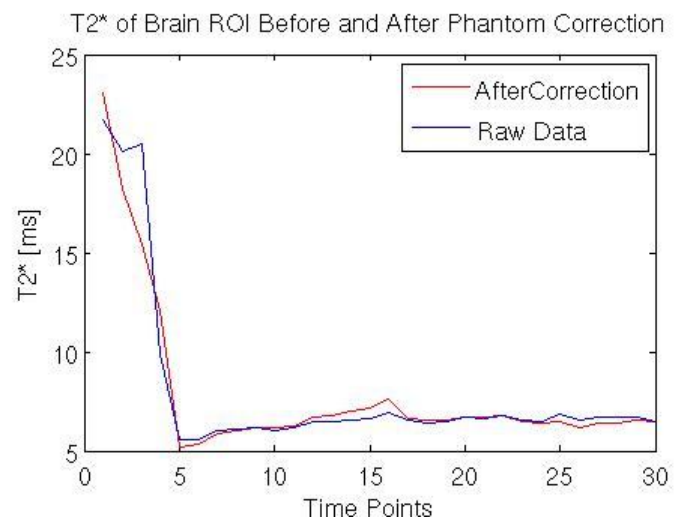
4.1.4 Reference Phantom Method
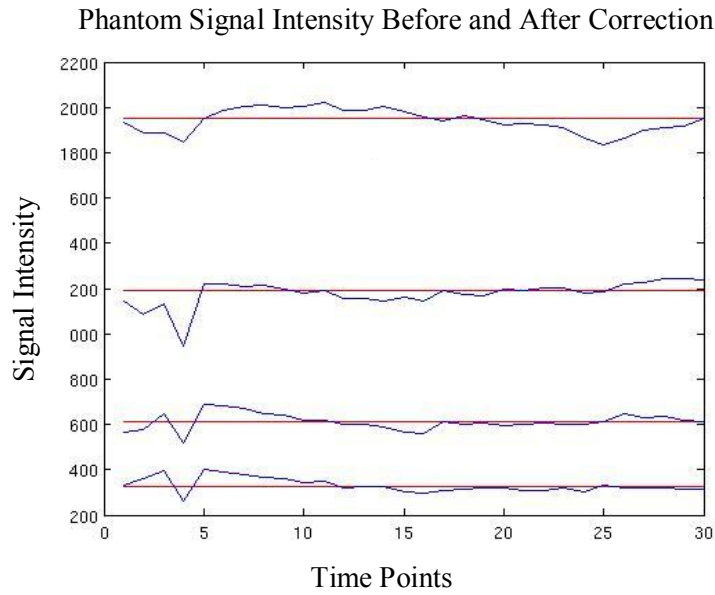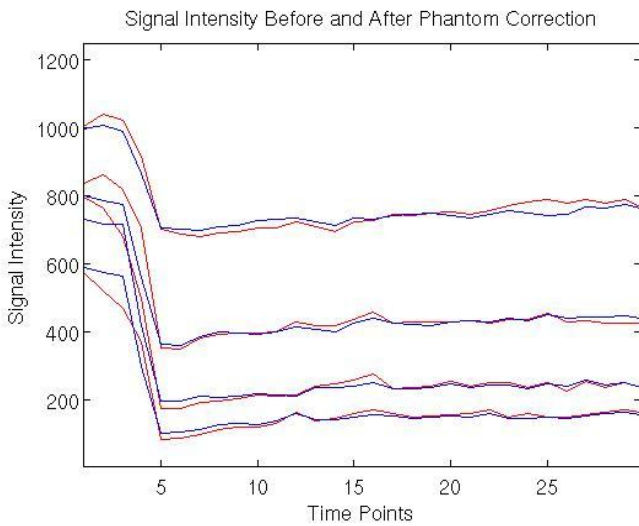
Figure 4. 8 Correction of thermal drift by external reference phantom. (a) Phantom signal intensities (raw data in blue and corrected data in red). (b) One pixel's raw(blue curve) and corrected signal intensities(red curve). (c) T2* based on raw data and corrected data.

Figure 4. 8 shows the thermal stability correction by an external reference phantom inside animal ear. Raw phantom signal intensities have a big variation at around time point 5 when CA was injected (Figure 4. 8 (a)). This may result from animal motion at that moment. After multiplying the correction matrix, the phantom signal intensities was corrected to be stable over time, but it is not the same case for a randomly selected pixel in brain area. Neither the intensities nor T_2* of that pixel were stabilized after correction. Therefore, the external reference phantom cannot remove the thermal drift as expected.
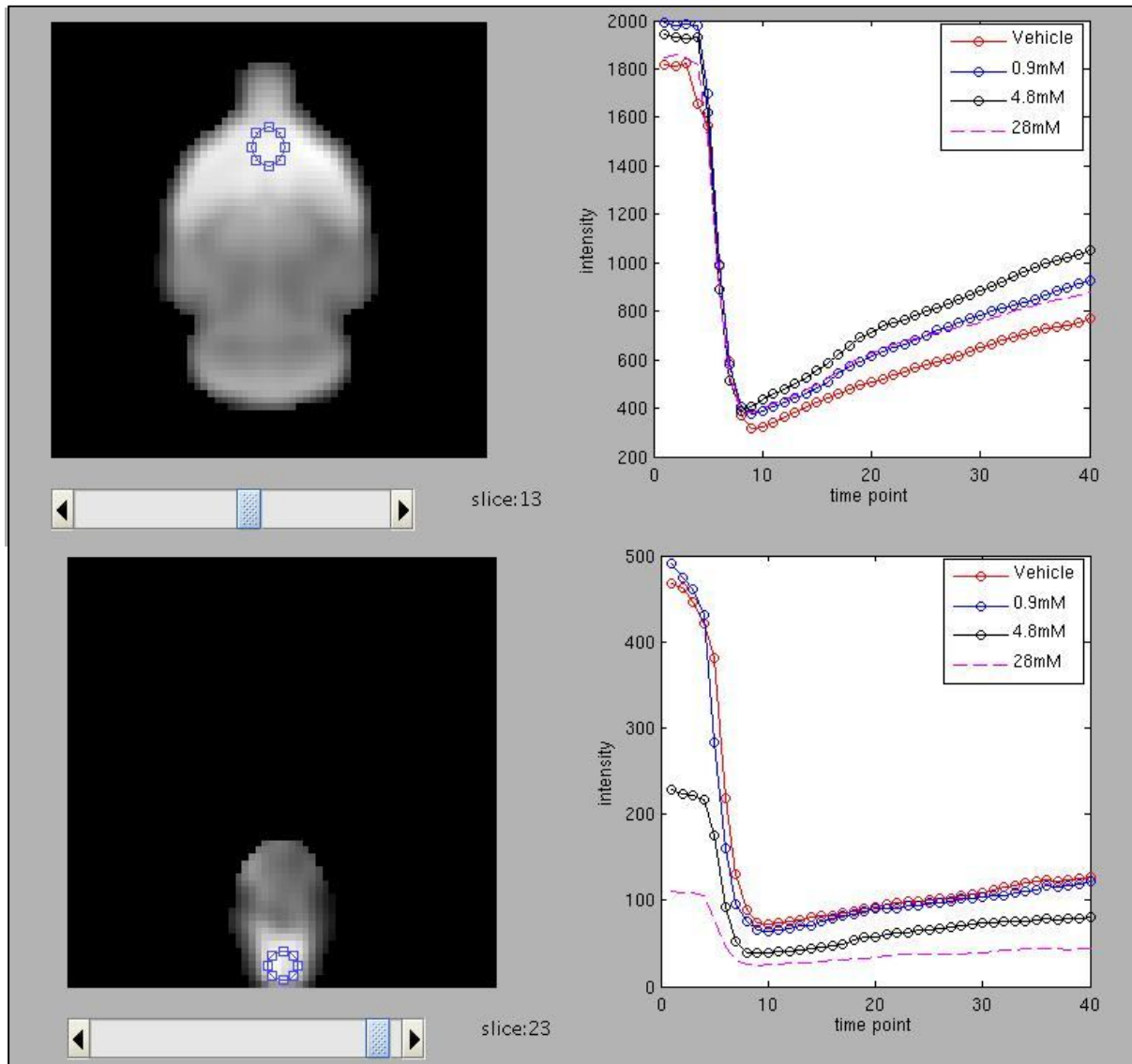
31

4.2 SPM Spatial Processing

Figure 4. 9 Two examples of mean time- signal intensity curves in different ROIs for dataset A.

After spatial processing by SPM, the brain volumes were smoothed and normalized. For dataset A, the signal intensities in two different ROIs of all the four groups (vehicle and three doses groups) are shown in Figure 4. 9. It is obvious that, in the first ROI, the vehicle group has a stable pattern over time while all the three treated groups have a hump at around time point 20, which is the compound injection time. This difference indicates a compound effect. However in the other ROI, signal intensities time course have the same tendency, where no different trend can be observed. This also implies that the compound has a local effect in certain brain region instead of a global impact.

4.3 T$_2$* Map Generation

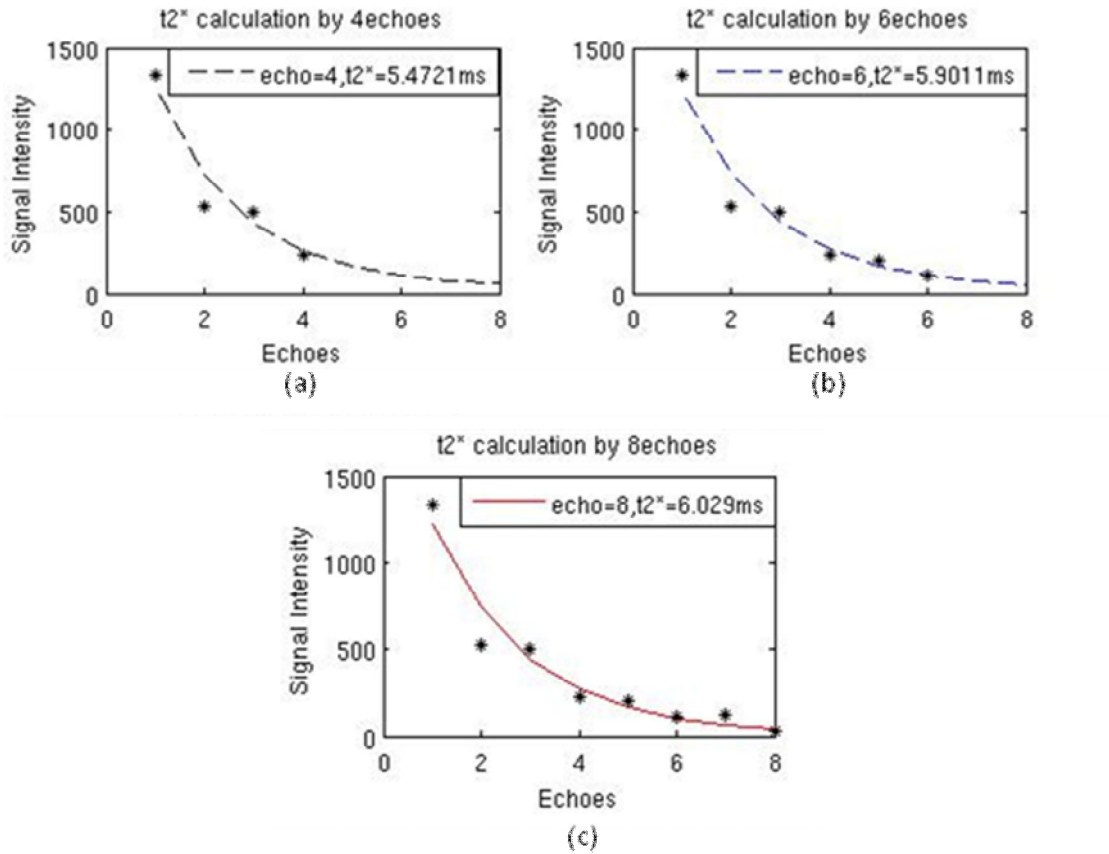It can be seen in the Figure 4.8 that T$_2$* values vary in fittings by different echoes.

Figure 4. 10 T$_2$* curve fitting by different echoes. (a) T$_2$* curve fitted on first 4 echoes (b) T$_2$* curve fitted on first 6 echoes. (c) T$_2$* curve fitted on 8 echoes.

To optimize the number of echoes to be acquired in the scanners, 60 pixels inside one animal's brain were randomly selected in one time point and T$_2$* curve-fitting was done on the first four, six and eight echoes for each pixel. Mean square error (MSE) was used as a metrics for the T$_2$* fitting qualify.

It can be seen in the Figure 4. 10 and Table 2 that the MSE of curve-fitting based on 4 echoes and 8 echoes are always larger than that with 6 echoes, which means the best fitting was performed by 6 echoes.

Table 2
Statistical qualification of T$_2$* fitting by different echoes

	Sum of square error in curve-fitting by 4 echoes	Sum of square error in curve-fitting by 6 echoes	Sum of square error in curve-fitting by 8 echoes
Mean value	74.4	54.1	55.9
Mean square error	47.1	34.8	36.1

4.4 Location of the Activated Regions

Data analysis results need to be thresholded to get the most significant regions by a proper p-value. Uncorrected (unc.) p-value and Family-wise Error (FWE) rate are two extend voxel-level thresholds for statistical analysis. FWE is also called corrected p-value, which is the probability of making one or more false discoveries among all the hypotheses when performing multiple pair-wise tests. FWE is a threshold for higher statistical significance than unc. p-value.
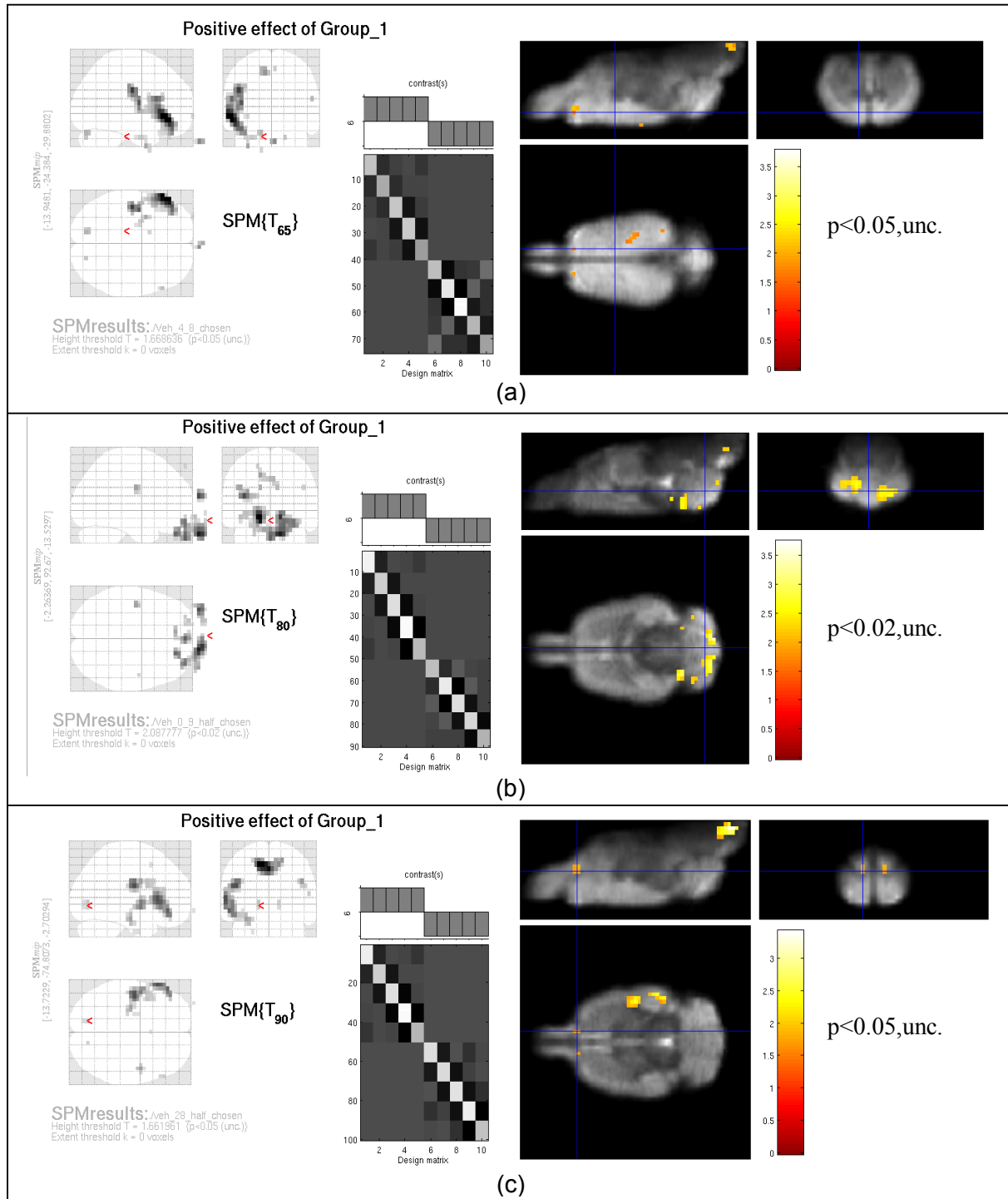
4.4.1 Time-bin Method

Figure 4. 11 Activation maps from Time-bin method by SPM of dataset A. (a) Vehicle group versus 0.9mM group. (b) Vehicle versus 4.0mM. (c) Vehicle versus 28mM.
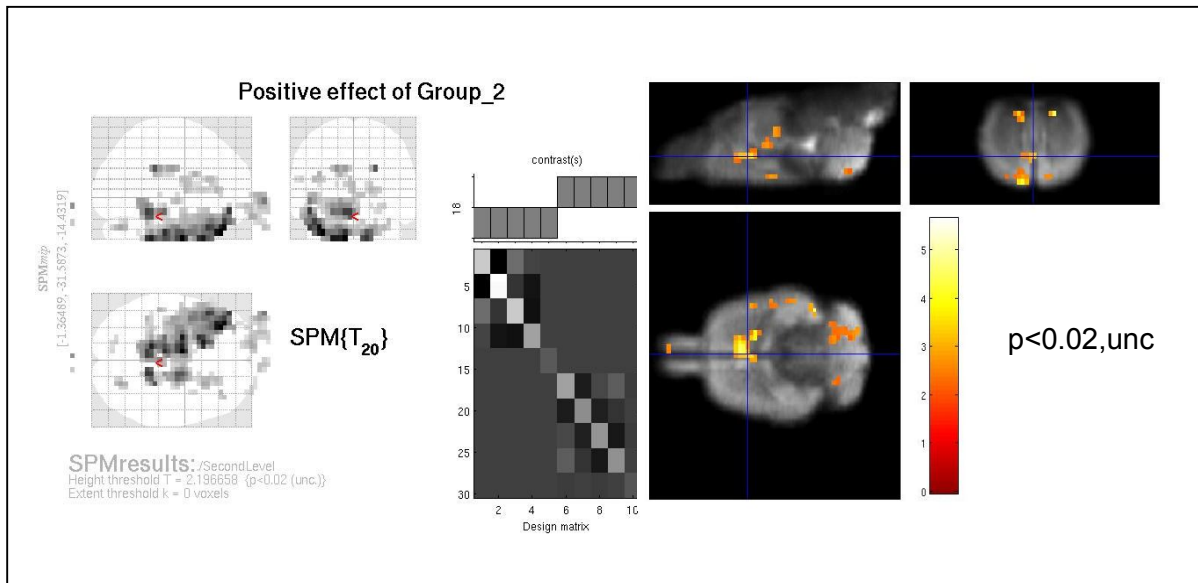
Figure 4. 12 Activation map from Time-bin method by SPM of the dataset B

Figure 4. 11 shows the results of Time-bin method by SPM on the dataset A. Three comparisons among low-dose (a), middle-dose (b), high-dose (c) and vehicle groups separately were done. The contrast 'Positive effect of Group_1' was selected, which means that the signal intensity in significant regions in the vehicle group recovers faster than in the compound groups. The threshold p-value used is around 0.05, unc. It can be seen that each comparison leads to different activated regions, although the same compound was used in each group. This indicates together with the high p-value, that the activation map may not be reliable.

Figure 4. 12 shows the activation map of the dataset B. Vehicle and compound groups were compared, and the contrast was opposite of 'Positive effect of Group_1', which means the compound increases T2* values in the significant regions. However, the activation map is not symmetric and the threshold p-value (p<0.02, unc) is much higher than commonly accepted p-value (p<0.05, FEW), which indicates that the result have to be evaluated with great caution. One possible reason is that the number of animals in the dataset B is low (3+3), which may not be enough for reliable analysis.

4.4.2 Shuffle Method

Shuffle method was applied only on the dataset A. Figure 4. 13 shows histograms of two randomly selected pixels by sorting their reshuffled T-values in an ascending order:
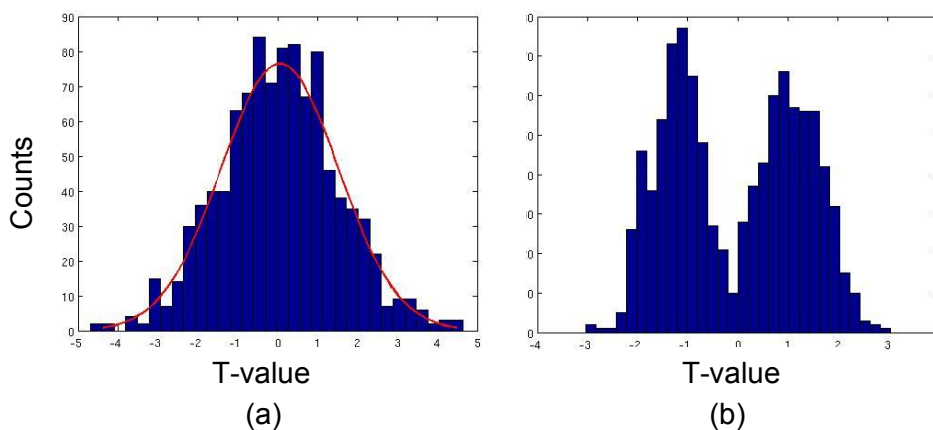

(a)   (b)

Figure 4. 13 Histogram of two randomly selected pixels' shuffled T-values. (a) Histogram of one pixel's shuffled T-values. (b) Histogram of the other pixel.

35

The histograms are the real distribution functions of these two pixels. It can be seen that the distribution function in the left follows quite close to true student's t-distribution (red curve) which is the assumption in the SPM analysis. But the pixel in the right follows no standard distribution.

Figure 4. 14 shows the inverse p-value map from the shuffle method. Brighter regions mean more significant response.
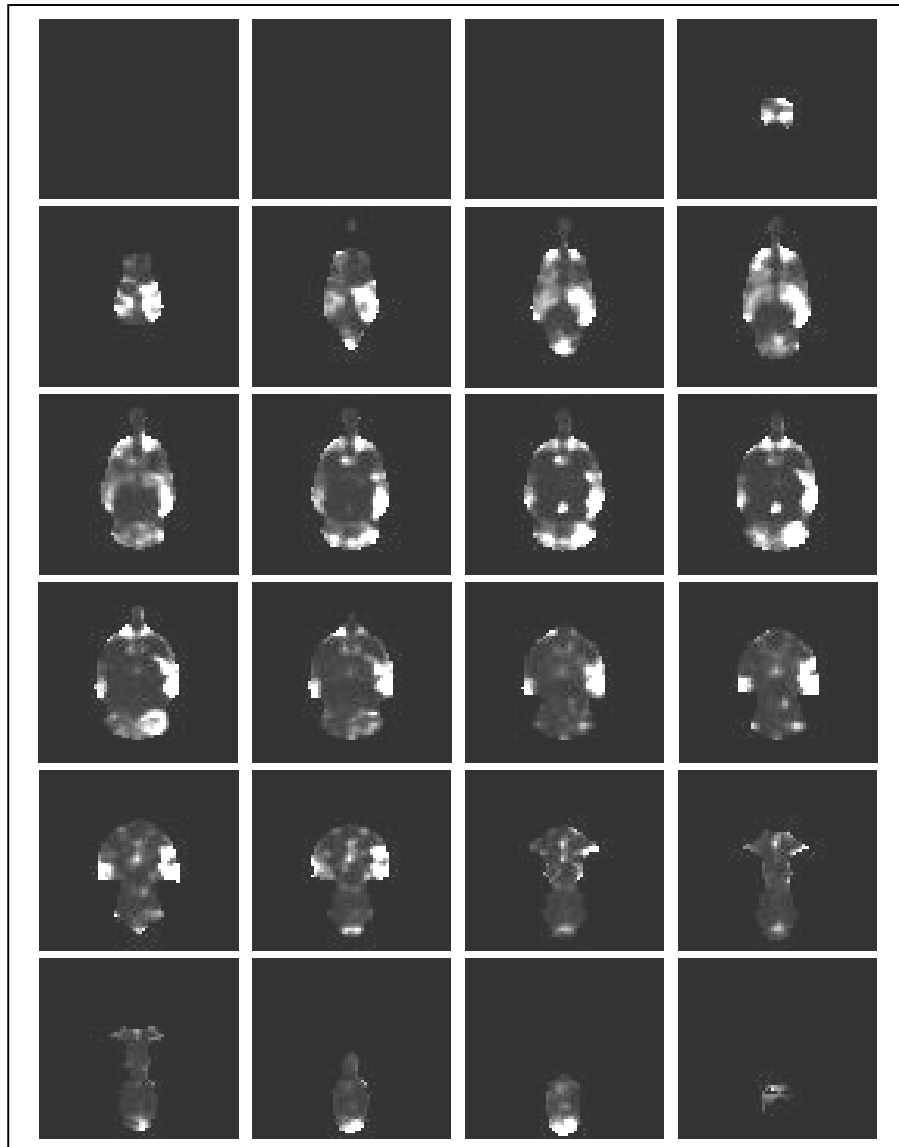

Figure 4. 14 Inverse p-value map from shuffle method. Bright regions indicate high probability that the vehicle and compound groups behave differently.

There are activations in the regions close to the anatomic regions where they are expected, such as hypothalamus. However, the large activations close to brain boundaries are unexpected, which may have been caused by motion and other reasons as well. Additionally, the p-values in the bright regions are much higher than the standard significant threshold (0.05, FWE), which means they cannot be considered as statistically significant.

4.4.3 Clearance Model Method

4.4.3.1 Clearance Model:
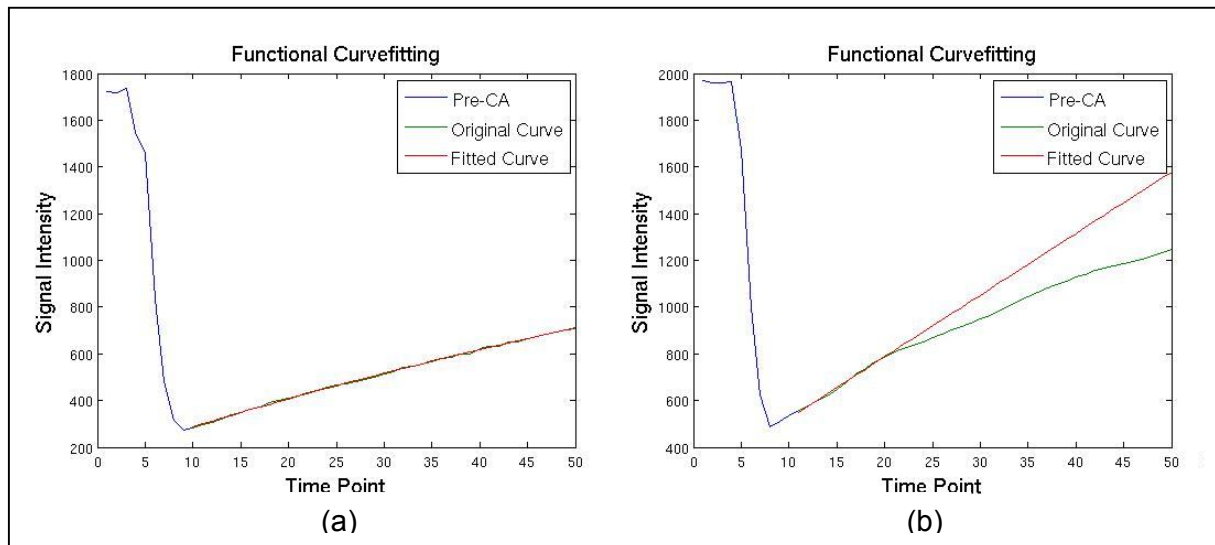1) Functional Model:

Figure 4. 15 (a) Functional curve fitting for the vehicle group. (b) Functional curve fitting for one treated group

Functional curve fitting of vehicle group (Figure 4. 15 (a)) utilized data of all the time points, while fitting of compound group was done between time points 11 to 20 (Figure 4. 15 (b)). The result of vehicle curve fitting is more accurate comparing to fitting of compound group with limited time points.

To detect that how many time points are needed for an accurate functional curve fitting, increasing number of time points were used to fit a curve and calculated the clearance, i.e, with 8, 13 to 29time points. The curve fitting with data of 29 time points was considered as the most accurate result and used as a reference. In Figure 4. 16, the clearance of each time interval is displayed. It shows that a clearance with 19 time points or more is stable and close to the result when all time points are included (29 time points), which indicates that functional fitting needs at least half of the total time points to be accurate.
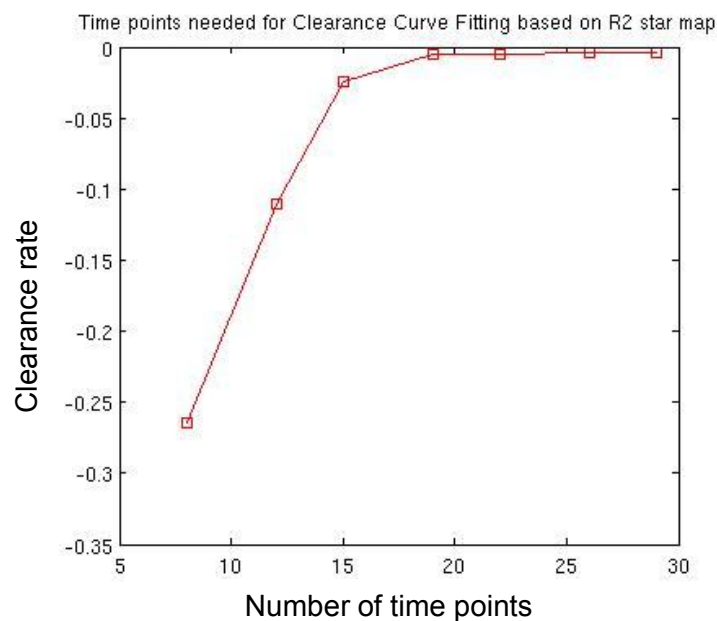

Figure 4. 16 Clearance rates computed by different number of time points for dataset B.

37

2) Numerical Model:

Figure 4. 17shows the standard clearance curves obtained from the dataset A vehicle animals (left), and from the dataset B vehicle animals (right).
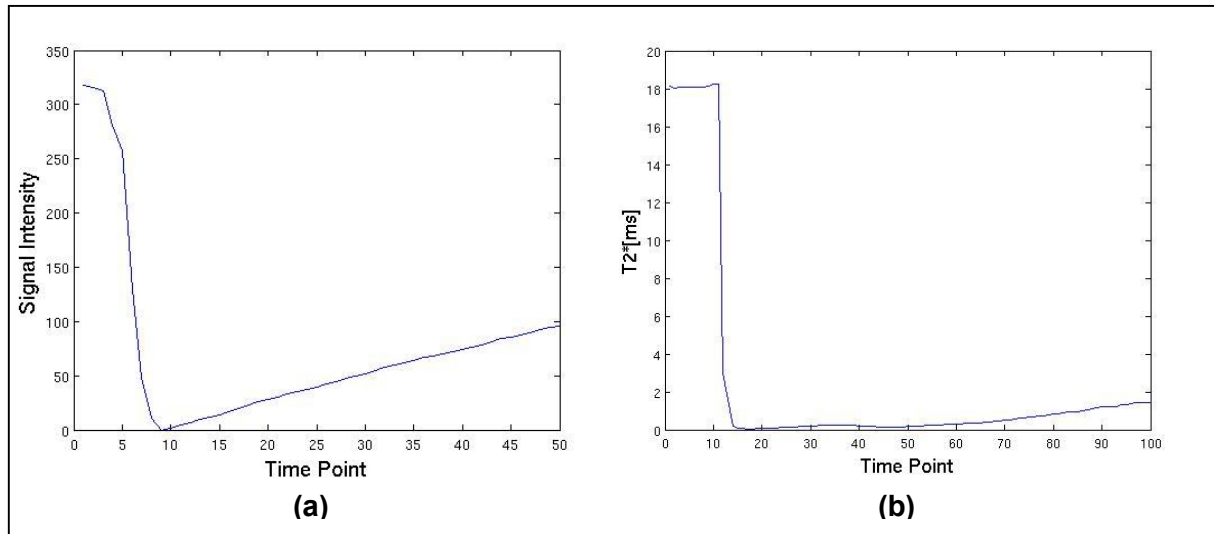
Figure 4. 17 Standard clearance curves from the dataset A (a) and dataset B (b). Note that in the Figure(a) the vertical axis is signal intensity while in the Figure (b) it is T2*.

Figure 4. 18 shows two pixels' time courses together with the matched standard clearance curves. The curves are matched to the time point 11 to 20. It can be seen that the matching has been successful in both cases and also that there is a deviation between the original two matched curves at last time points. This is used in a statistical analysis to find a compound effect.
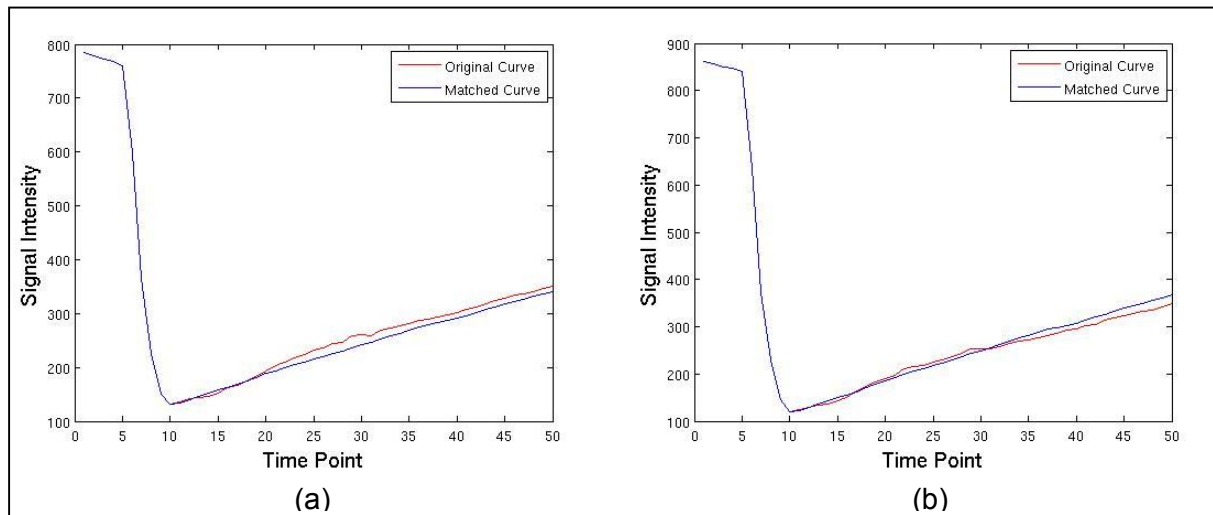
Figure 4. 18 Linearly fit the standard clearance curve (blue) to single pixel's time curve (red) from a treated animal.

4.4.3.2 Clearance curve matching and Time-bin Method

For the dataset A, the comparison of all the treated groups (three doses) with the sample group result is displayed in Figure 4. 19 (p< 0.05, FWE).The activations have high left-right symmetry and the activated sites form a highly structured pattern. There is also an activated region in the brain stem where this compound is known to have receptors.

Figure 4. 19 Activation map by using clearance curve matching and time-bin method between sample and treated group of dataset A (p<0.05, FWE).

For dataset B, Time-bin analysis displays the difference between sample and compound group in Figure 4. 20 (p<0.05, FWE). It can be observed that the structure has a relative symmetry but it is not perfect, possibly because of the small amount of animals in this dataset.
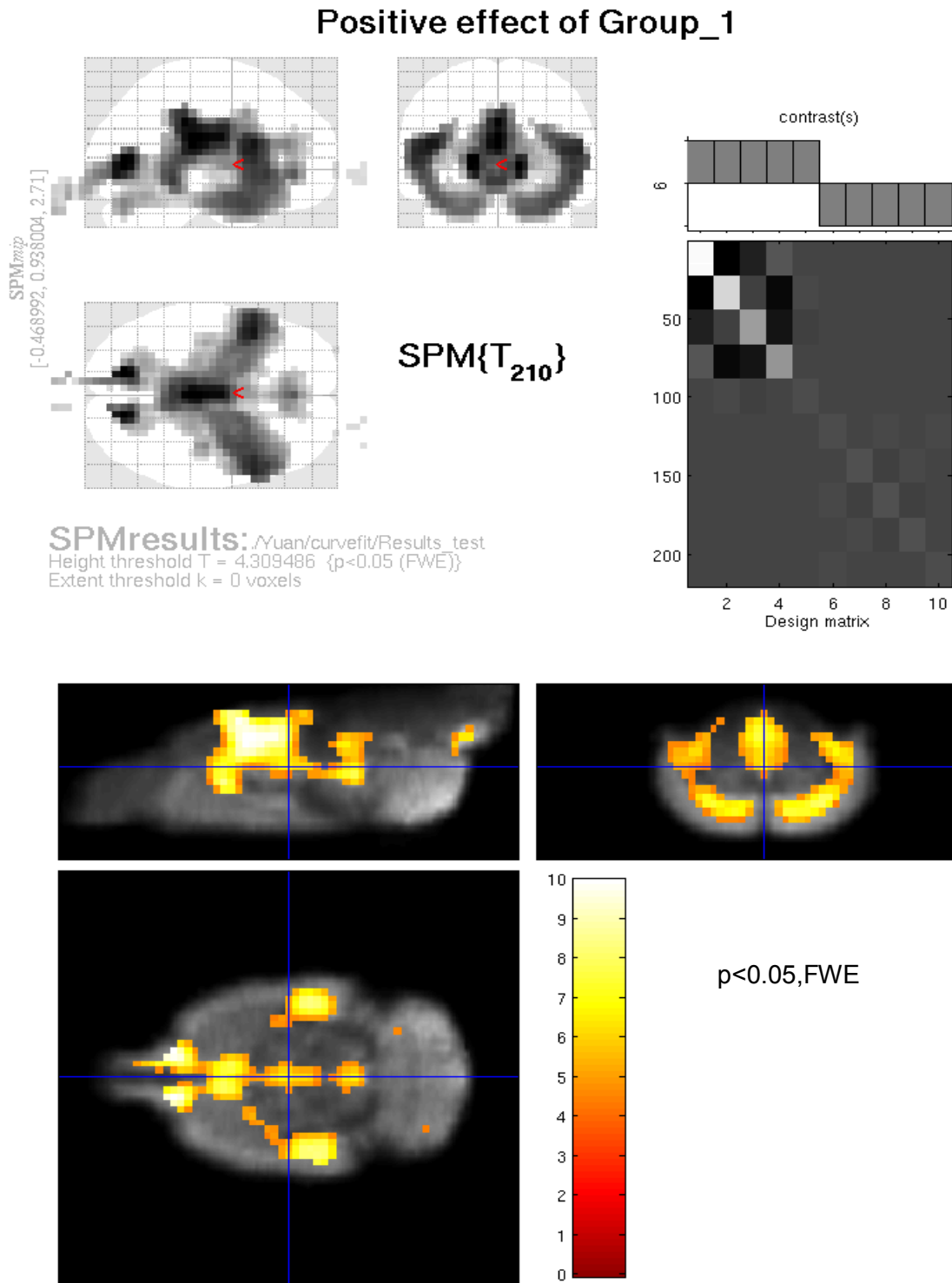

Figure 4. 20 Activation map by using clearance curve matching and time-bin method between sample and treated group of dataset B (p<0.05, FWE).

In order to test the dose effect from dataset A, the same method was used for group comparison tests between each dose group and its sample group separately.

In Figure 4. 21, (a), (b) and (c) are the results from low-dose to high-dose groups. The activation maps are not exactly equal and some dose groups show stronger response than the others. However, all the three maps show activations in similar regions. This is a further indication that the activation map in Figure 4. 19 is correct. Thus it can be trusted as the real activated regions which happened in all the dose cases.
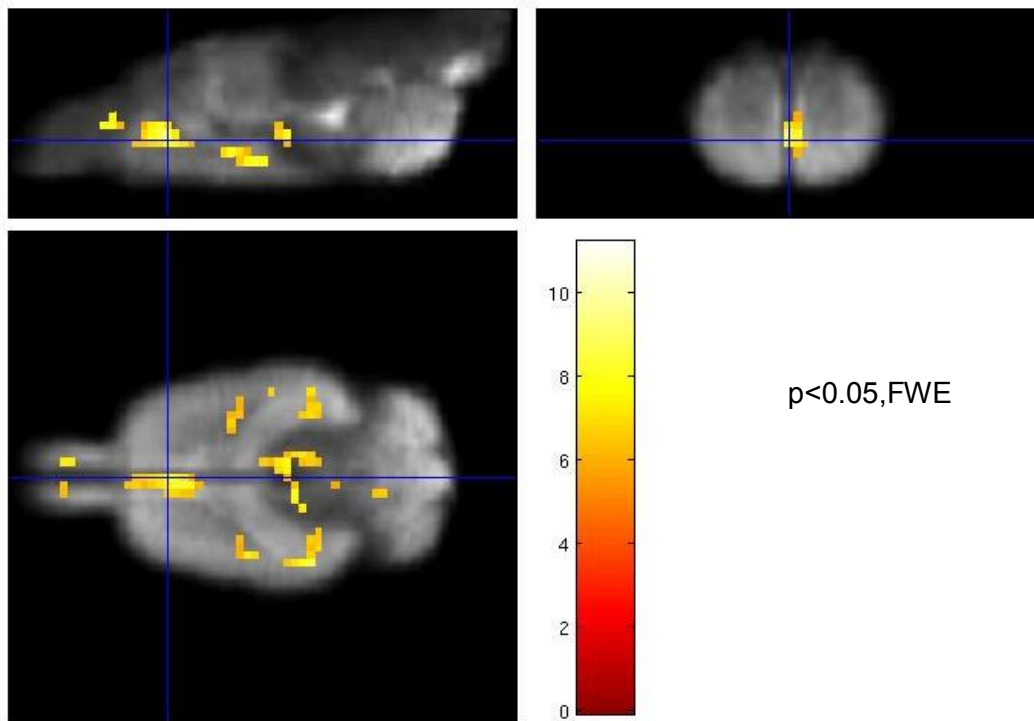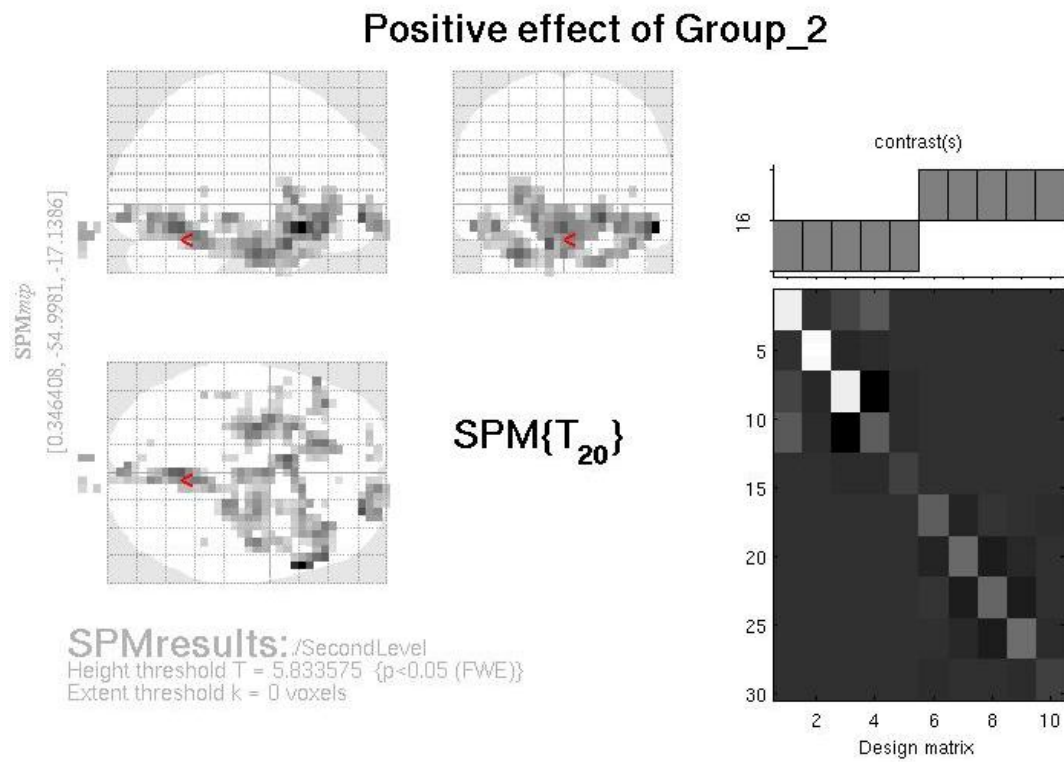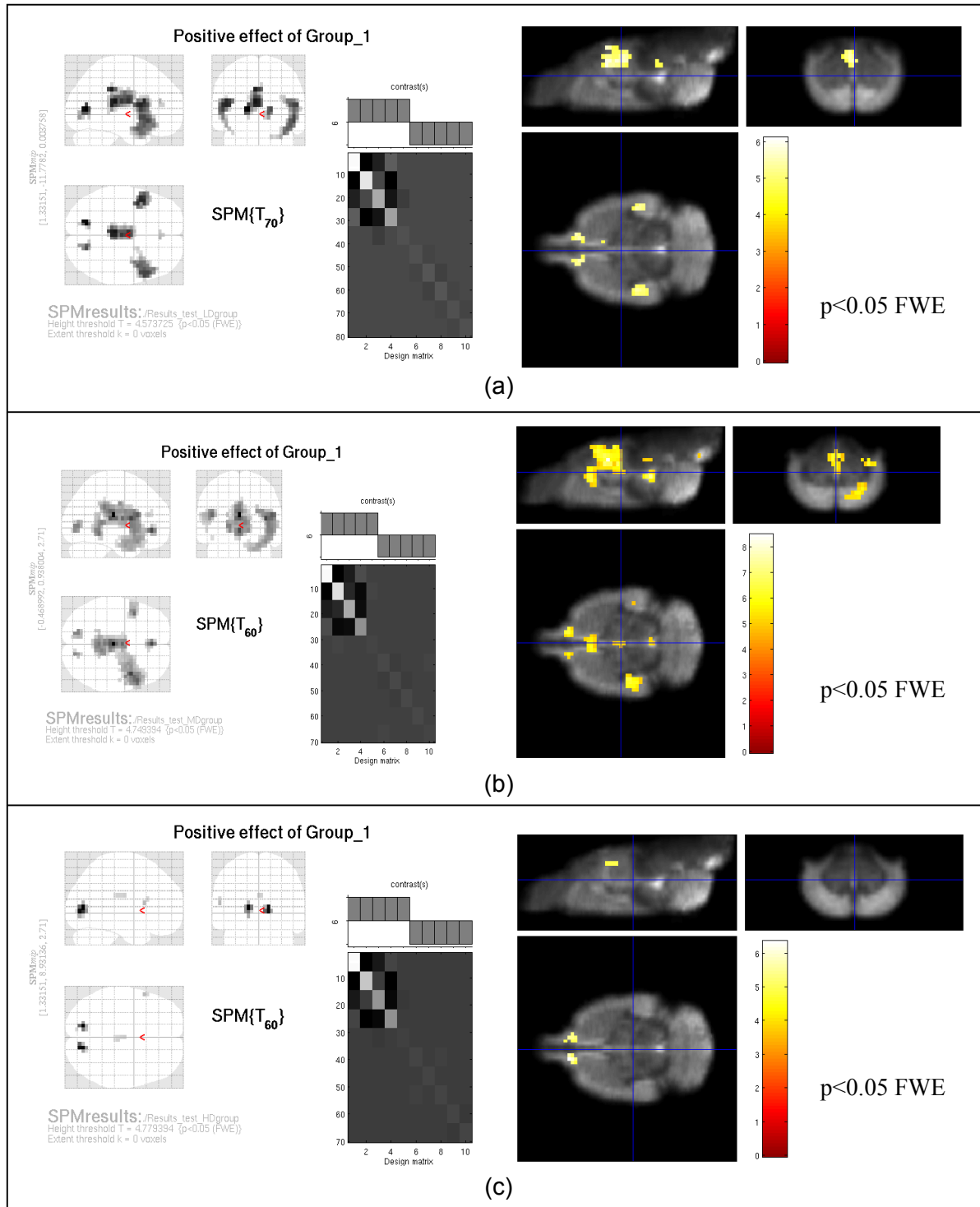

Figure 4. 21 Activation maps of different doses by using clearance curve matching and time-bin method between sample and treated group of dataset A. (a) Group comparison result for dataset A, 0.9mM. (b) Group comparison result for dataset A, 4.8mM. (c) Group comparison result for dataset A, 28.0mM.

4.4.3.3 Clearance curve matching and extraction

Clearance curve extraction method was applied to dataset A. Figure 4. 22 shows the horizontal slices of a rat brain template where in white are the highest activation regions which were threshold by p<0.05 (FWE). The activated regions are very close to the results of Time-bin analysis (Figure 4. 19).
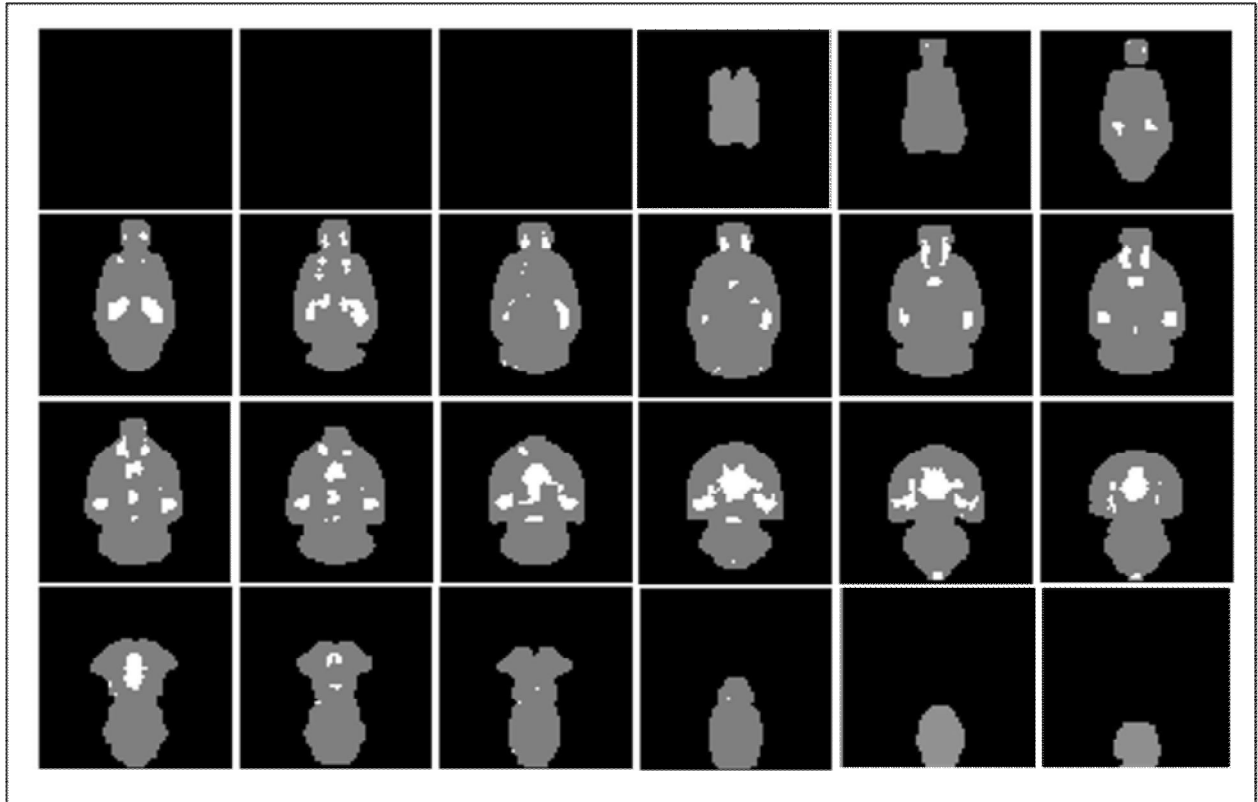
Figure 4. 22 Activation map of the dataset A which was analyzed by clearance-curve matching and extraction method. White regions indicate significant (p<0.05 FWE) activated areas. Gray regions are the horizontal slices of a rat brain template.

4.5 Quantification — ΔrCBV Calculation

The group-level ΔrCBV-time curve from the activated regions (Figure 4. 22) of dataset A is shown in Figure 4. 23. It can be seen that all the curves ascend after time point 20, because the time points (11 to 20) used for matching were limited. During time points after 21, ΔrCBV in the low-dose group is similar as the vehicle and middle-dose group is systematically higher than all the other groups. The high-dose group's ΔrCBV rises above the low-dose group after time point 21 but stays all the time below the middle-dose's curve.
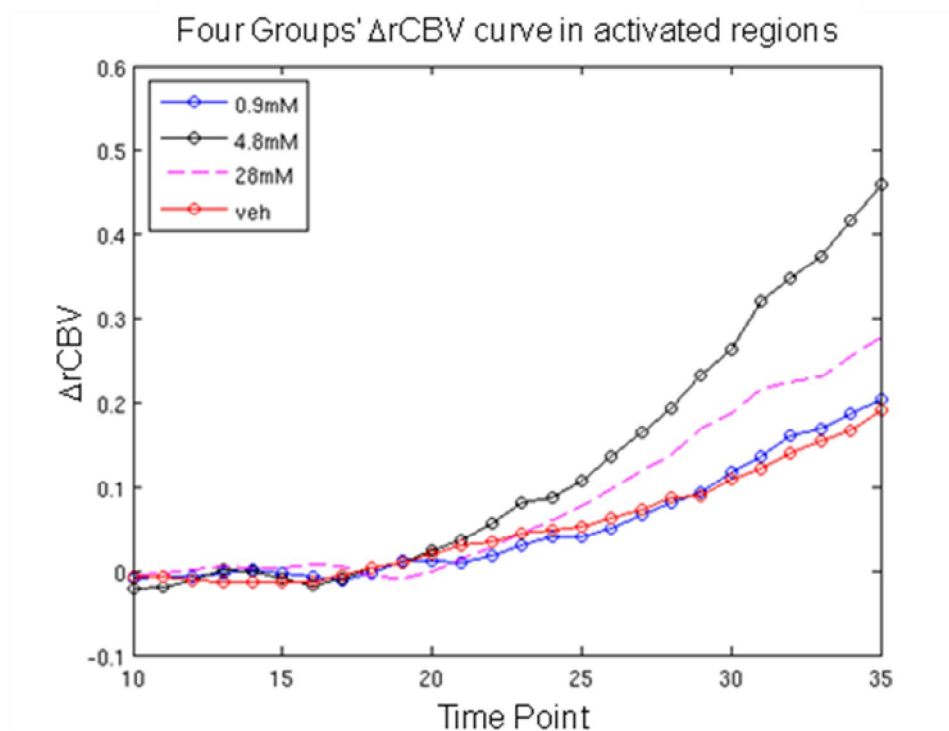

Figure 4. 23 Mean ΔrCBV of brain activation regions in all groups of dataset A.

The inaccuracy of curve matching leads to unacceptable high ΔrCBV value for the last several time points. For comparing the dose effect, time interval 21 to 30 which is as long as the pre-substance period were used to calculate the mean ΔrCBV for each group.

Table 3
Dose effect of dataset A.

Dose Group	Mean ΔrCBV of activated regions [%]	receptor occupancy [%]
0.9mM	5	50
4.8mM	13	90
28mM	9	>100

Receptor occupancy [(29)] is the ratio between the amount of drug bounded receptors and total number of active receptors. The relationship between receptor occupancy and response (ΔrCBV) is expected to be linear. Table 3 shows the quantifications of responses and corresponding receptor occupancies for all the treated groups. The ΔrCBV result does not totally follow the expectation. The low-dose and middle-dose groups' results follow the increasing tendency, but the effect of the high-dose group is negative might because of over-dose.

Chapter 5 **Discussion**

The purpose of this work was to locate the drug-induced brain activation regions and to quantify the dose effects based on pharmacoMRI dataset in terms of signal intensity and T_2*. The whole work can be divided into two parts: Data processing and statistical analysis.

In the data processing part, the attempt was to correct the signal intensity variations introduced by motion and field inhomogeneity, which was tested by four approaches. Among them, the filter method was applied to both dataset A and B; the rigid-body and overlay method were tested for the dataset A only, and the external reference phantom was used on the dataset B.

The filter method intends to use a proper filter to smooth the time-intensity curves for each pixel in all the animals' brains. Bilateral filter can basically fulfill the request but it turns out to eliminate some of the useful information as well. Thus, it has a limited usefulness for both dataset A and B.

The rigid-body method was relied on the hypothesis that two objects will have similar coil sensitivity patterns if the same scan configurations were used. This approach combines the information from SPM and ParaVision. SPM realignment estimation contains all the rigid-body transformation parameters, and all the scan configuration parameters and raw data are stored in ParaVision. The basic procedure is to calculate the animal motion from SPM rigid-body parameters, to locate corresponding voxel positions before and after motion correction in a uniform reference phantom and to compensate the intensity ratio back to the brain. However, finding the animals' motion from the SPM realignment parameters was not successful. There are two possible reasons for this: Firstly it is possible that not only 6-digit rigid-body transformation is applied to the data, but also the signal intensities are modified by the SPM during the reslice or interpolation procedures. The SPM motion correction files contains also zooms and shears parameters which may be related to the size change and rotation, and these parameters have not been taken into account in the rigid-body transformation matrix that developed in this work. Secondly, reslicing, which is the next step after realignment, uses an interpolation algorithm to re-sample the image signal intensity.

An experiment (Figure 4. 3 and Figure 4. 4) was implemented by finding the motion explicitly from the raw data instead of using the SPM motion correction information. This experiment was successful, which indicates that the rigid-body method is reasonable if real voxel positions and intensities are found in space and the hypothesis of this method is promising. However, it requires finding the animals' motion manually from the raw data, which is not feasible for large dataset. Thus, the rigid-body method was not implemented. In the future, if an automatic tool can be developed to find the motion and intensity information from the raw data correctly, this can be a highly accurate method to correct the motion-induced signal intensity.

In the overlay method, the same assumption is made as in the rigid-body method— two objects will have similar coil sensitivity patterns with the same scan configuration. Rather than the complex computations from the SPM realignment parameters, only raw data was used here. After finding the overlapping regions of brain and the uniform reference phantom in a common coordinate system, the signal intensities in brain overlapping regions were divided by the reference phantom. In this way, the field inhomogeneity effects were eliminated. This method requires phantom large enough to cover all the main brain regions, so that the intensity variation caused by the animal's head-motion can always be corrected by the overlay method. The overlay method is the most successful one of all the data processing approaches tested, and it was applied to the dataset A in prior to all the statistical analysis tested.

The external phantom method to correct system drift was applied on dataset B. The signal intensities and T_2* after the correction had a higher variation than original values. The possible reason is that the animal has moved. The assumption that the phantom signal intensity is stable when system drift is eliminated is not correct. The animals did not tolerate the silicon reference phantom in the ear, and the method was abandoned before sufficient amount of data had been collected for a thorough analysis.

For the statistical analysis, Time-bin method, shuffle method, and clearance model method were tested.

The activation maps from the vehicle and compound groups' comparison by using the Time-bin method show regions with relatively low left-right symmetry and insignificant p-value both in dataset

A and B. One reason is that, the data is assumed to follow the student t-distribution in SPM statistics, which is not the real case in the dataset A. Thus, the Time-bin method applied on this type of data is not recommended, unless the dataset contains a large amount of animals.

In order to obtain the true distribution for individual pixels, a shuffle method was used on the dataset A. The results indicate that the shuffle method may improve the SPM analysis results as seen by the increased level of symmetry, and significant activations appear in deep brain regions which are known to be involved as appetite regulation. The drawback was the artifacts emerging at the edge of the brain, which were unexpected and possibly not real activation.

Both of the analysis methods above compared treated groups with vehicle group based on the assumption that the vehicle group can stand for the clearance curve for all the treated animals. This is not entirely correct as each animal has its own ability to clear the contrast agent, and therefore its own clearance curve. To increase the sensitivity and accuracy of the statistical analysis, the clearance model method was developed to obtain the real clearance curve for each animal. Functional and numeral methods were used to find out the individual clearance.

Functional approach was based on a mono-exponential curve fitting. However, the contrast media in this study has a very long washout time, which results in a slow decay and the numerical value of the decay constant is small. It brings in inaccuracy to the curve-fitting algorithm, especially to the T_2* data. Furthermore, there were only few pre-substance time points in the treated group which could be used for estimation, which was not enough for an efficient curve-fitting. In the substance period, the extrapolated curve had therefore a tendency to deviate a lot from the original curve. The functional curve fitting was therefore deemed as not a successful method to obtain the clearance curve when the numbers of time points can be used are few.

The numeral method generates a standard clearance model based on the average of all the vehicle animals, and then the model was linearly matched to the compound subjects' curves in the pre-substance period. The matched curve excludes the compound effect and is tailored for the individual treated animal. It can be observed that numerical method is superior to the functional curve fitting to obtain the clearance curves for treated animals, as the matched clearance curve has a much less bias from original curve compared to the functional fitted one.

The matched clearance curves generated the sample group for analysis. The Time-bin analysis applied on the sample group and the treated group improved the activation map evidentially. For the dataset A, the activation map is highly symmetrical. The statistic significance of the activated regions is high ($p<0.05$, FWE). For the dataset B, the activation map is not as perfect as dataset A with some artifacts, but the symmetry is relatively high and the p value is standard ($p<0.05$, FWE). The comparison between sample group and treated group was found to be a very sensitive method to locate the brain activation areas. The only disadvantage of this method is that all the time points after the substance administration should be included to get enough data for SPM analysis, which means the last most untrusted values have also to be included.

The clearance curve extraction method based on the sample group and the treated group for the dataset A resulted in a clear activation map within the brain. This method uses one-sample t-test to obtain the activation map instead of using SPM analysis, and the result is more accurate. The requirement of this method is enough amounts of data, so that a t-test can be implemented.

Based on the activation map from the clearance curve extraction method on the dataset A, the ΔrCBV of the significant regions at all three doses were calculated. The findings were: substance A has an acute systematic effect, and when the dosage increases from low (0.9mM) to medium (4.0mM) to high dose (28mM), the ΔrCBV differences between treated groups could be seen. The ΔrCBV values do not linearly follow the dosages, as the highest value appear at the medium dose (4.0mM). There is no plateau found in the dose effects. More time points are needed for the pre-substance period to get a more accurate curve matching, and therefore more reliable clearance curves. For dataset B, more animals are needed for a better activation map, so the ΔrCBV calculation is in progress.

Bibliography

1. Rabi II, Zacharias JR, Millan S, and Kusch P. A new method of measuring nuclear magnetic moment. *Phys. Rev.* 53 (1938): 318.
2. Bloch F. Nuclear induction. *Phys. Rev.* 70 (1946): 460-473.
3. Purcell EM, Torrey HC, and Pound RV. Resonance absorption by nuclear magnetic moments in a solid. *Phys. Rev.* 69 (1946): 37.
4. Chen Q, Andersen AH, Zhang Z, Ovadia A, Gash DM, and Avison MJ. Mapping drug-induced changes in cerebral R2* by multiple gradient recalled echo functional MRI. *Magn Reson Imaging* 14 (1996): 469-476.
5. Chen YC, Mandeville JB, Nguyen TV, Talele A, Cavagna F, and Jenkins BG. Improved mapping of pharmacologically induced neuronal activation using the IRON technique with superparamagnetic blood pool agents. *J Magn Reson Imaging* 14 (2001): 517-524.
6. Constable RT. Challenges in fMRI and its limitations. In: *Functional neuroradiology: principles and clinical applications*, by Faro SH, Mohamed FB, Law M and Ulmer JT, 331-344. Springer Science and Business Media, 2011.
7. Belliveau JW, Kennedy DN, Mckinstry RC, Buchbinder BR, Weisskoff RM, Cohen MS, Vevea JM, Brady TJ, Rosen BR. Functional mapping of the human visual cortex by magnetic resonance imaging. *Science* 254 (1991): 716-719.
8. Sell LA, Simmons A, Lemmens GM, Williams SCR, Brammer M, and Strang J. Functional magnetic resonance imaging of the acute effect of intravenous heroin administration on visual activation in long-term heroin addicts: results from a feasibility study. *Drug and Alcohol Dependence* 49 (1997): 55-60.
9. Breiter HC, Gollub RL, Weisskoff RM, Kennedy DN, Makris N, Berke JD, Goodman JM; Kantor HL, Gastfriend DR, Riorden JP, Mathew RT, and Hyman SE. Acute effects of cocaine on human brain activity and emotion. *Neuron* 19 (1997): 591-611.
10. Gollub, RL, Kantor H, Kennedy D, Gastfriend D, and Mathew RT. Cocaine decreases cortical cerebral blood flow but does not obscure regional activation in functional magnetic resonance imaging in human subjects. *J Cereb Blood Flow Metab* 18 (1998): 724-734.
11. Li SJ, Biswal B, Li Z, Risinger R, and Rainey C. Cocaine administration decteases functional connectivity in human primary visual and motor cortex as detected by functional MRI. *Magn Reson Med.* 43 (2000): 45-51.
12. Jacobsen LK, et al. Impact of intravenous nicotine on BOLD signal response to photic stimulation. *Magn Reson Imaging* 20 (2002): 141-145.
13. Lawrence NS, Ross TJ, and Stein EA. Cognitive mechanisms of nicotine on visual attention. *Neuron* 36 (2002): 539-548.
14. Laurienti PJ, Field AS, Burdette JH, Maldjian JA, Yen YF, and Moody DM. Dietary caffeine consumption modulates fMRI measures. *NeuroImage* 17 (2002): 751-757.
15. Mulderink TA, Gitelman DR, Meulam MM, and Parrish TB. On the use of caffeine as a contrast booster for BOLD fMRI studies. *NeuroImage* 15 (2002): 37-44.
16. Meyer JH, Kennedy S, and Brown GM. No effect of depression on [15O]H2O PET response to intravenous d-fenfluramine. *Am J Psychiatry* 155 (1998): 1241-1246.
17. Lahti AC, Holcomb HH, Medoff DR, and Tamminga CA. Ketamine activates psychosis and alters limbic blood flow in schizophrenia. *Neuroreport* 6 (1995): 869-872.
18. Grasby PM, Friston KJ, Bench CJ, Cowen PJ, and Frith CD. The effect of the dopamine agonist, apomorphine, on regional cerebral blood flow in normal volunteers. *Psychol Med.* 23 (1993): 605-612.
19. Christoforidis GA, Bourikas EC, Baujan M, Abduljalil AM, Kangarlu A, Spigos DG, Chakeres DW, and Robitaille ML. High resolution MRI of the deep brain vascular anatomy at 8 tesla: susceptibility-based enhancement of the venous structures. *J comput Assist Tomogr* 23 (1999): 857-866.
20. Truong TK, Chakeres DW, Beversdorf DQ, Scharre DW, and Schmalbrock P. Effects of atatic and radiofrequency magnetic field inhomogeneity in ultra-high field magnetic resonance

imaging. *Magn Reson Imaging* 24 (2006): 103-112.

21. Friston KJ, Williams S, Howard R, Frackowiak RS, and Turner R. Movement-related effects in fMRI time-series. *Magn Reson Med.* 35 (1996): 346-355.

22. Bennett EP, and McMillan L. Video enhancement using per-pixel virtual exposures. *ACM Trans. Graph.* 24, no. 3 (2005).

23. Chadwick M and Sebastian C. Co-registration and Spatial Normalisation. *Wellcome Trust Centre for Neuroimaging.* 2008.　　http://www.fil.ion.ucl.ac.uk/spm/doc/mfd/2008/norm.ppt.

24. Gearing O and Kelly J. SPM pre-processing. *Wellcome Trust Centre for Neuroimaging.* 2004. http://www.fil.ion.ucl.ac.uk/spm/doc/mfd/2004/preprocessing.ppt.

25. Kiebel SJ, Ashburner JA, Poline JB, and Friston KJ. MRI and PET Coregistration—A cross validation of statistical parametric mapping and automated image registration. *Neuroimage* 5 (1997): 271-279.

26. Ashburner J, and K J Friston. Chapter 2- Rigid body registration. In: *Human Brain Function*, eds: Ashburner J, Friston KJ and Penny W, 2-18. 2003.

27. Alexander L. 2nd level analysis-design matrix, contrasts and inference. *Wellcome Trust Centre for Neuroimaging.* 2008.
http://www.fil.ion.ucl.ac.uk/~jchumb/powerpoint%20presentations/SPM%202nd%20level%20analysis.ppt.

28. Henriksson L. Visualization and quantification of fMRI results. *BRU/LTL and AMI, Helsinki University and Technology.* 2009.
http://ltl.tkk.fi/wiki/images/1/18/Henriksson_fMRI09_visuquan.pdf.

29. Piascik MT. *Receptor Workbook.* University of Kentucky. 2005.
http://www.mc.uky.edu/pharmacology/instruction/pha824mp/pha824mp.html.

30. Hornak JP. *The basics of MRI.* http://www.cis.rit.edu/htbooks/mri.

31. Loepprich M. *Coordinate system.* 2011.
http://www.slicer.org/slicerWiki/index.php/Coordinate_systems.